Report

Cell Reports

Flvcr1a deficiency promotes heme-based energy metabolism dysfunction in skeletal muscle

Graphical abstract

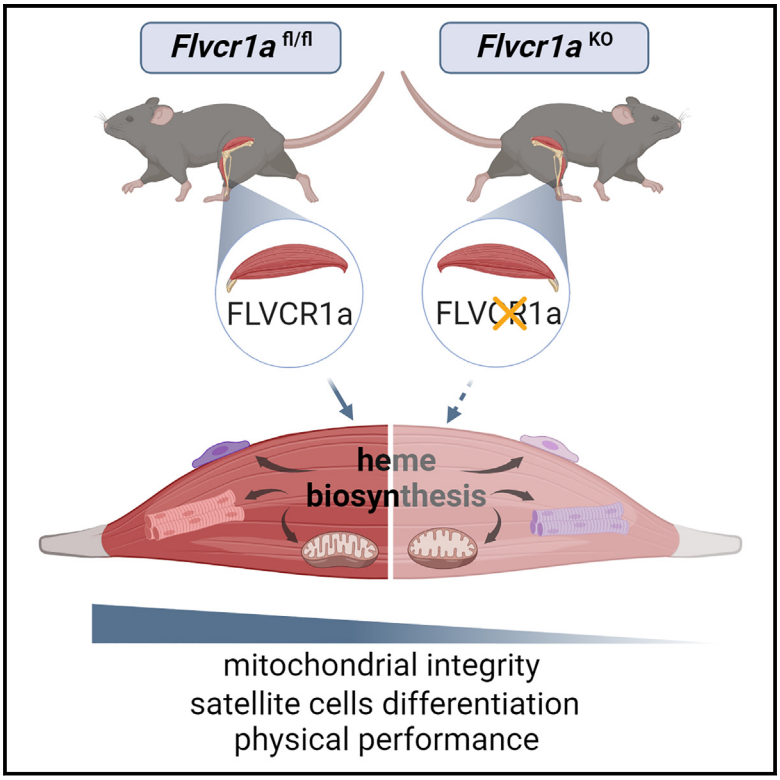

Highlights

- FLVCR1a loss in skeletal muscle impairs tissue features and physical performance
- FLVCR1a tunes heme synthesis, impacting myofiber identity and mitochondrial function
- By sustaining heme synthesis, FLVCR1a controls satellite cell differentiation

Authors

Miriam Mistretta, Veronica Fiorito, Anna Lucia Allocco, ..., Chiara Riganti, Yvan Torrente, Emanuela Tolosano

Correspondence

yvan.torrente@unimi.it (Y.T.), emanuela.tolosano@unito.it (E.T.)

In brief

Controlling metabolic pathways vital for muscle function and regeneration is a promising strategy to counteract muscle disease. Here, Mistretta and Fiorito et al. analyze the consequences of FLVCR1a deficiency in skeletal muscle and demonstrate that, by sustaining heme synthesis, FLVCR1a shapes myofiber energy phenotype and regulates satellite cell differentiation.

Mistretta et al., 2024, Cell Reports *43*, 113854
March 26, 2024
https://doi.org/10.1016/j.celrep.2024.113854

CellPress

Cell Reports

CellPress
OPEN ACCESS

Report

Flvcr1a deficiency promotes heme-based energy metabolism dysfunction in skeletal muscle

Miriam Mistretta,[1,10] Veronica Fiorito,[2,10] Anna Lucia Allocco,[2] Giorgia Ammirata,[2] Myriam Y. Hsu,[2] Sabrina Digiovanni,[3] Marzia Belicchi,[4] Laura Napoli,[5] Michela Ripolone,[5] Elena Trombetta,[6] PierLuigi Mauri,[7,8] Andrea Farini,[1] Mirella Meregalli,[4] Chiara Villa,[4] Paolo Ettore Porporato,[2] Barbara Miniscalco,[9] Simonetta Geninatti Crich,[2] Chiara Riganti,[3] Yvan Torrente,[1,4,11,*] and Emanuela Tolosano[2,11,12,*]

[1]Neurology Unit, Fondazione IRCCS Ca' Granda Ospedale Maggiore Policlinico, 20122 Milan, Italy
[2]Molecular Biotechnology Center (MBC) "Guido Tarone", Department of Molecular Biotechnology and Health Sciences, University of Torino, 10126 Torino, Italy
[3]Molecular Biotechnology Center (MBC) "Guido Tarone", Department of Oncology, University of Torino, 10126 Torino, Italy
[4]Stem Cell Laboratory, Department of Pathophysiology and Transplantation, Dino Ferrari Centre, Università degli Studi di Milano, 20122 Milan, Italy
[5]Neuromuscular and Rare Diseases Unit, Department of Neuroscience, Fondazione IRCCS Ca' Granda Ospedale Maggiore Policlinico, 20122 Milan, Italy
[6]Flow Cytometry Service, Clinical Pathology, Fondazione IRCCS Ca' Granda Ospedale Maggiore Policlinico, 20122 Milan, Italy
[7]National Research Council of Italy, Proteomics and Metabolomics Unit, Institute for Biomedical Technologies, ITB-CNR, 20054 Segrate, Milan, Italy
[8]Clinical Proteomics Laboratory c/o ITB-CNR, CNR.Biomics Infrastructure, ElixirNextGenIT, 20054 Segrate, Milan, Italy
[9]Department of Veterinary Sciences, University of Torino, 10095 Grugliasco, Torino, Italy
[10]These authors contributed equally
[11]These authors contributed equally
[12]Lead contact
*Correspondence: yvan.torrente@unimi.it (Y.T.), emanuela.tolosano@unito.it (E.T.)
https://doi.org/10.1016/j.celrep.2024.113854

SUMMARY

The definition of cell metabolic profile is essential to ensure skeletal muscle fiber heterogeneity and to achieve a proper equilibrium between the self-renewal and commitment of satellite stem cells. Heme sustains several biological functions, including processes profoundly implicated with cell metabolism. The skeletal muscle is a significant heme-producing body compartment, but the consequences of impaired heme homeostasis on this tissue have been poorly investigated. Here, we generate a skeletal-muscle-specific feline leukemia virus subgroup C receptor 1a (FLVCR1a) knockout mouse model and show that, by sustaining heme synthesis, FLVCR1a contributes to determine the energy phenotype in skeletal muscle cells and to modulate satellite cell differentiation and muscle regeneration.

INTRODUCTION

Regulating metabolic pathways essential for muscle functions is emerging as a promising strategy to counteract skeletal muscle disease progression or to potentiate the innate ability of skeletal muscle to regenerate. Skeletal muscles display diverse metabolic compositions, matching energy needs with contractile demands. This diversity extends to satellite cells (SCs), a designated population of muscle stem cells,[1] highlighting the importance of mitochondrial metabolism in balancing their self-renewal and commitment during muscle recovery upon injury.[2]

Feline leukemia virus subgroup C receptor 1a (FLVCR1a) is a ubiquitously expressed membrane transporter. Traditionally recognized as a heme exporter,[3] recent works[4–7] proposed that it may alternatively/additionally import choline. Both heme and choline metabolism play pivotal roles in processes that provide energy to cells. Consequently, the modulation of FLVCR1a's function could potentially impact skeletal muscle energetic metabolism. Furthermore, previous studies have shown that FLVCR1a participates in a common functional axis with δ-aminolevulinic acid synthase 1 (ALAS1),[8–10] the rate-limiting enzyme for heme synthesis, thereby affecting metabolic pathways dependent on heme and/or interconnected with ALAS1, including the tricarboxylic acid (TCA) cycle.[8]

Here, by using skeletal-muscle-specific *Flvcr1a*-null mice, we demonstrate that FLVCR1a is a critical determinant of skeletal muscle metabolism required for proper muscle function and regeneration.

RESULTS

FLVCR1a loss in skeletal muscle reduces heme biosynthesis

To evaluate the impact of FLVCR1a loss in skeletal muscles, we generated skeletal-muscle-specific *Flvcr1a*-knockout (*Flvcr1a*^{KO}) animals (Figure S1A). As *Flvcr1a* is equally expressed in

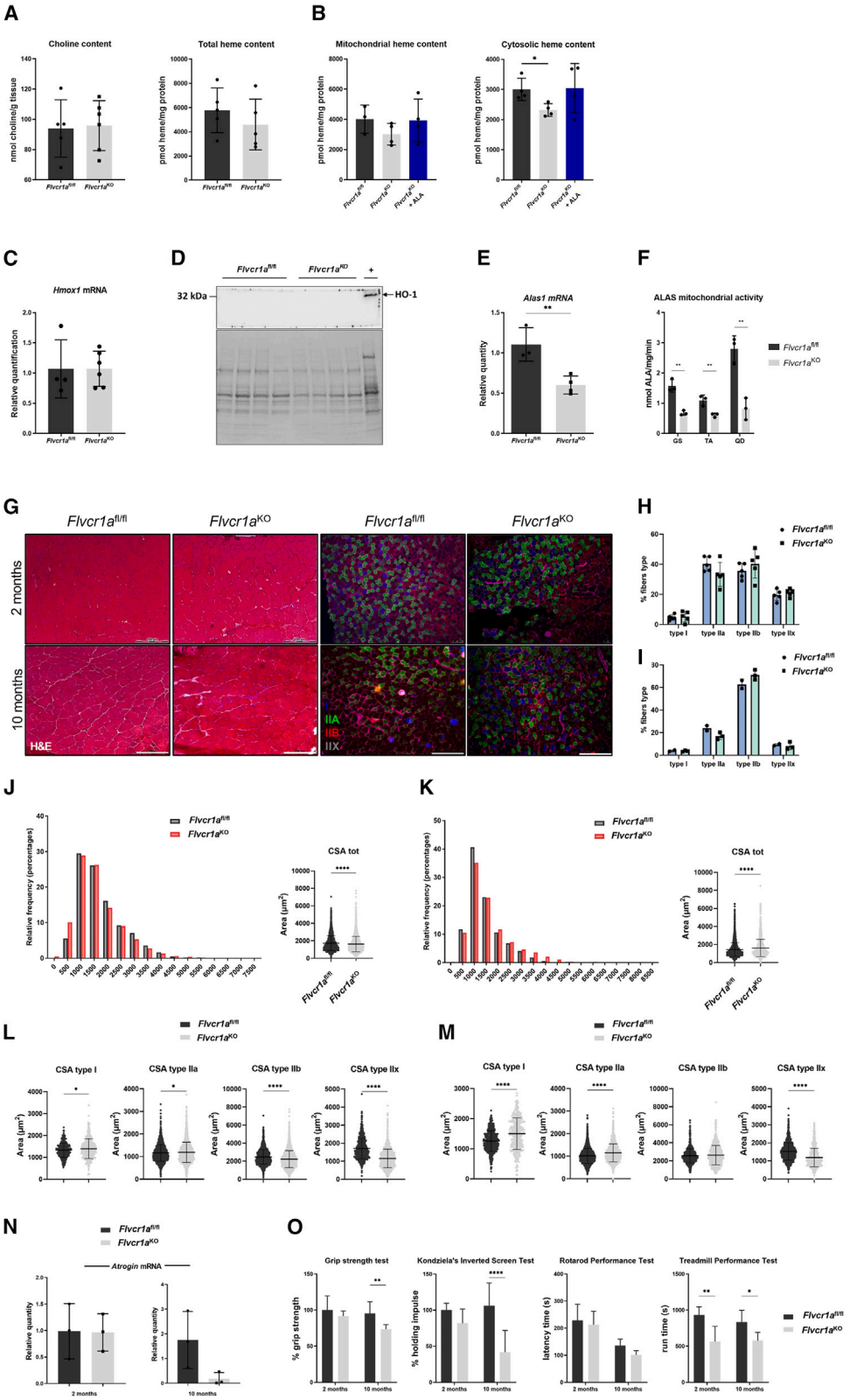

(legend on next page)

gastrocnemius (GS), tibialis anterior (TA), and quadriceps (Figure S1B), deletion efficiency was assessed on GS. We detected a 90% decrease in the *Flvcr1a* transcript (Figure S1C), whereas protein amount was reduced by 50% (Figure S1D) in the entire skeletal muscle, a level consistent with the heterogeneous composition of whole-tissue lysates. *Flvcr1a*^{KO} offspring were obtained at the expected mendelian ratio (Figures S1E and S1F) and exhibited normal activity, motility, lifespan, and body weight (Figures S1G and S1H).

Given the ongoing debate regarding FLVCR1a's function as either a choline importer or a heme exporter, we analyzed both GS choline and heme levels. Free choline quantity was comparable in *Flvcr1a*^{KO} and control samples (Figure 1A), indicating that the lack of FLVCR1a does not impact choline homeostasis, at least under the steady-state and experimental conditions examined. Consequently, our attention shifted to heme.

Any disruptions in heme homeostasis exert a selective pressure, favoring cells capable of activating compensatory mechanisms to maintain heme at a tolerable level. As a result, if present, minimal changes in heme levels were expected in the muscle of our mice, posing a challenge for detection using available techniques. We detected a comparable overall heme quantity in *Flvcr1a*^{KO} and *Flvcr1a*$^{fl/fl}$ total GS lysates (Figure 1B) but a trend decrease in the mitochondrial fraction and a significant slight reduction in the cytosolic fraction (Figure 1B).

Although the limited sensitivity of the techniques employed for heme detection, and the modest decrease in heme quantity measured in a single-cell compartment, did not provide conclusive information on alterations in heme homeostasis in our model, this result suggested to us the possibility of perturbed heme in *Flvcr1a*^{KO} muscle. Therefore, we conducted a more comprehensive examination of potential dysregulation in heme metabolism in *Flvcr1a*^{KO} mice by investigating both heme degradation and synthesis. The expression of the inducible heme-degrading enzyme heme oxygenase 1 (HO-1; encoded by the *Hmox1* gene) was unaffected in *Flvcr1a*^{KO} GS (Figure 1C). Moreover, HO-1 protein was not detected in western blot analyses in *Flvcr1a*$^{fl/fl}$ GS, as expected in the absence of a trigger for HO-1 induction, and a similar result was obtained in *Flvcr1a*^{KO} GS (Figure 1D). Conversely, heme biosynthesis was compromised, as *Alas1* mRNA levels (Figure 1E) and ALAS mitochondrial activity (Figure 1F) were significantly reduced in *Flvcr1a*^{KO} muscle. Reinforcing this observation, oral treatment of *Flvcr1a*^{KO} mice with 5-aminolevulinic acid (ALA), a well-known agent capable of inducing *de novo* heme synthesis bypassing ALAS1, reversed the declining trend in mitochondrial heme levels and corrected the slight cytosolic heme deficiency (Figure 1B).

Together, these findings suggest that the lack of FLVCR1a results in the reduction of heme biosynthesis.

FLVCR1a loss results in deranged myofibers features and reduced overall muscle performance

To evaluate the morphological consequences of FLVCR1a loss, we performed histological analyses. We did not observe inflammatory cells, collagen deposition, or the accumulation of fat in transverse sections from *Flvcr1a*^{KO} GS (Figure 1G), soleus (SOL) (Figure S2A), and TA (Figure S3A). Although the numbers of muscle fibers and percentages of fiber types were comparable among *Flvcr1a*^{KO} and *Flvcr1a*$^{fl/fl}$ mice (Figures 1H, 1I, S2B, S2C, S3B, and S3C), the cross-sectional area (CSA) of GS myofibers was significantly reduced in 2-month-old KO mice (Figure 1J). Conversely, we observed a shift toward larger myofiber CSAs in the GS of 10-month-old *Flvcr1a*^{KO} mice when compared to controls (Figure 1K). The analysis of myofiber-type-specific CSAs in GS showed distinct patterns. Specifically, type I and IIa fibers, which are known for their oxidative characteristics, exhibited an overall increase in CSA, whereas type IIb and IIx fibers, which are glycolytic, showed a reduction in CSA (Figures 1L and 1M). Remarkably, 10-month-old *Flvcr1a*^{KO} mice showed larger oxidative fibers in SOL (Figures S2D–S2G) and smaller glycolytic fibers in TA (Figures S3D–S3G). In summary, *Flvcr1a*^{KO} mice show atrophy of glycolytic fibers and hypertrophy of oxidative fibers. These effects become more pronounced in older mice and are particularly prominent in muscles that primarily rely on

Figure 1. FLVCR1a loss in skeletal muscle reduces heme biosynthesis and results in deranged myofiber features and decreased overall muscle performance

(A) Free choline and heme content measured in whole GS lysates.
(B) Heme content measured in GS mitochondrial and cytosolic fractions at the steady state and after ALA.
(C) Real-time RT-qPCR analysis of GS *Hmox1* expression.
(D) Western blot analysis of GS HO-1 protein level. A representative image is shown. As a positive control, the amount of HO-1 protein in a fibrotic liver is displayed on the right side of the filter. Stain-free total protein measurement[11] is included as the loading control.
(E) Real-time RT-qPCR analysis of GS *Alas1* expression.
(F) ALAS mitochondrial activity measured in TA, GS, and quadriceps (QD).
(G) Representative images of H&E staining and immunofluorescence of myosin heavy chain (blue: type I, green: type IIa, red: type IIb, black: type IIx) in GS of 2- and 10-month-old mice.
(H and I) Mean percentage of myofibers types in GS of 2- (H) and 10-month-old (I) mice.
(J and K) Relative frequency distribution of myofibers CSA in GS of 2- (J) and 10-month-old (K) mice. In the bean plots, the CSAs of all the myofiber types are reported.
(L and M) CSAs of myofibers in 2- (L) and 10-month-old (M) mice, grouped by myosin heavy-chain types.
(N) Real-time RT-qPCR analysis of GS *Atrogin* expression.
(O) Motor behavior tests to assess strength (grip and Kondziela's), coordination (rotarod), and endurance (treadmill).
Scale bar: 200 μm (G). Group averages were compared using unpaired Student's t test (A–C, E, F, and J–N), two-way ANOVA test (H and I), and one-way ANOVA test (O). *$p < 0.05$, **$p < 0.01$, and ****$p < 0.0001$. Data are presented as mean ± SD with n = 5 (*Flvcr1a*$^{fl/fl}$) or 6 (*Flvcr1a*^{KO}) mice (A, choline content) and n = 5 mice/group (A, total heme content); n = 4 mice/group (B and D); n = 4 (*Flvcr1a*$^{fl/fl}$) or 6 (*Flvcr1a*^{KO}) mice (C); n = 3 (*Flvcr1a*$^{fl/fl}$) or 4 (*Flvcr1a*^{KO}) mice (E); n = 3 mice/group (F, I, K, M, and N); n = 5 mice/group (H, J, and L); n = 8–10 mice/group (grip test, Kondziela's, rotarod); and n = 4–8 mice/group (treadmill) (O).
See also Figures S1–S3.

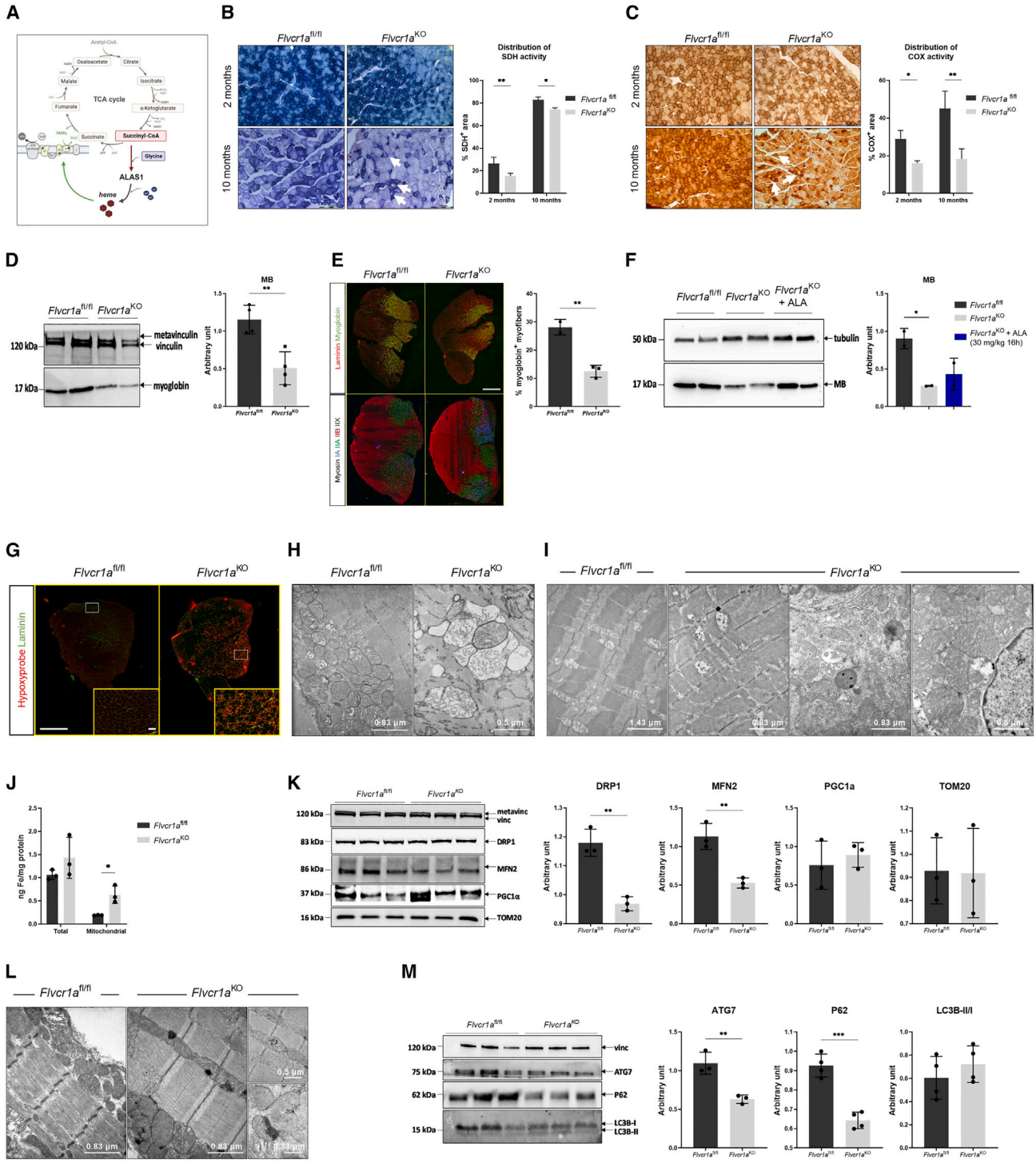

Figure 2. FLVCR1a loss affects muscle fiber metabolism, myoglobin expression, and mitochondrial integrity

(A) Schematic showing ALAS1's role in heme biosynthesis and cellular energy metabolism. Created with BioRender.com.

(B and C) Staining and quantification of GS succinate dehydrogenase (SDH) (B) and complex IV (COX) (C) distribution of enzymatic activity.

(D) Western blot analysis of GS myoglobin protein level. A representative image is shown, with vinculin expression as a loading control. Band intensities were measured by densitometry and normalized to vinculin expression.

(E) Representative images of distribution and composition of GS myosin heavy-chain isoforms (type I, type IIa, type IIx, and type IIb) (bottom) and immunofluorescence staining of myoglobin (red) and laminin (green) (top). The graph shows the percentage of myoglobin-expressing myofibers.

(legend continued on next page)

glycolytic or oxidative metabolism, respectively. In agreement with CSA analysis, the mRNA expression of atrogin in GS was decreased in 10-month-old mice only (Figure 1N).

The impact of CSA changes on motor performance was then assessed. Young *Flvcr1a*^{KO} mice did not show any difference in strength compared to age-matched control mice, whereas older *Flvcr1a*^{KO} mice showed a significant reduction (Figure 1O). Motor coordination was unchanged at 2 months of age but slightly reduced at 10 months of age (Figure 1O). Finally, endurance to exercise was reduced at both 2 and 10 months of age (Figure 1O).

In conclusion, motor performance is compromised in muscles lacking FLVCR1a, with a significant age-dependent decline, underscoring the essential role of FLVCR1a in maintaining lifelong muscle homeostasis.

Flvcr1a loss affects muscle fiber metabolism and myoglobin expression

Energy metabolism plays a pivotal role in shaping the identity of muscle fibers,[2,12,13] and a decrease in heme biosynthesis can exert a substantial and opposite influence on cellular energy metabolism, as heme biosynthesis acts not solely as a source of heme but also as a cataplerotic pathway for the TCA cycle (Figure 2A). Hence, to understand the underlying reason behind the compromised muscle morphology and performance in *Flvcr1a*^{KO} mice, we conducted a more comprehensive exploration of muscle metabolism. In line with the observed atrophy of glycolytic fibers in GS, the maximum activity of most glycolytic enzymes was lower in *Flvcr1a*^{KO} GS lysates than in controls (Figure S4A). Moreover, the maximum activity of some of these enzymes in young *Flvcr1a*^{KO} animals was reminiscent of an aged phenotype, being almost comparable to that of old control mice (Figure S4A). We confirmed the same trend in TA, prevalently composed by glycolytic fibers (Figure S4B). On the other hand, the maximum activity of most oxidative enzymes in GS mitochondrial fractions was higher in *Flvcr1a*^{KO} than in *Flvcr1a*$^{fl/fl}$ mice and showed an expected age-dependent decline, comparable to that of controls (Figures S4C and S4D). Since this measurement provided an average of the potential maximum enzyme activity across the entire tissue, we also measured the activities of electron transport chain (ETC) complexes II (succinate dehydrogenase [SDH]) and IV (COX) in GS cryosections to obtain a more accurate understanding of the actual extent of areas with elevated oxidative metabolism within the tissue. We observed quite restricted regions displaying positive staining for SDH and COX activity in *Flvcr1a*^{KO} mice (Figures 2B and 2C) and more extensive negative/slightly positive areas. The latter were especially expanded in 10-month-old *Flvcr1a*^{KO} mice, where even "white areas" were noticeable in some oxidative fibers (arrows in Figures 2B and 2C). Likewise, SDH and COX staining was also decreased in SOL (Figures S2H and S2I) and TA cryosections (Figures S3H and S3I). In summary, the data indicate that, despite maintaining the number of glycolytic fibers, *Flvcr1a*^{KO} muscles show atrophy of these fibers and reduced glycolytic metabolism. Moreover, *Flvcr1a*^{KO} muscle maintains the number of oxidative fibers, and these fibers exhibit a higher potential for sustaining oxidative phosphorylation (OXPHOS). However, only a small fraction of them can effectively execute OXPHOS. Therefore, it appears that *Flvcr1a*^{KO} muscle fibers are primed to be more oxidative but are unable to properly sustain OXPHOS.

We hypothesized that compromised OXPHOS in *Flvcr1a*^{KO} muscle was due to a potential decrease in oxygen supply. Previous studies have shown that, even when there are adequate intracellular heme levels, the presence of an active heme synthesis pathway that provides newly synthesized heme is crucial for the production of hemoproteins.[14] Therefore, decreased heme biosynthesis in *Flvcr1a*^{KO} mice could result in inadequate levels of myoglobin, the most important hemoprotein in skeletal muscle, responsible for oxygen storage and delivery.

To test this hypothesis, we analyzed myoglobin levels in *Flvcr1a*^{KO} skeletal muscle and detected a strong down-modulation on its amount, as well as a reduction in the percentage of myofibers expressing it (Figures 2D and 2E). Of note, these fibers co-localized with type I and type IIa myofibers (Figure 2E), which are known to be oxidative. Reduced myoglobin level in *Flvcr1a*^{KO} GS was restored, at least in part, by oral ALA treatment (Figure 2F), confirming that decreased heme biosynthesis accounted for it.

Consistent with decreased myoglobin production, we identified hypoxic regions selectively in *Flvcr1a*^{KO} myofibers (Figure 2G). The local hypoxia was likely due to reduced myoglobin,

(F) Western blot analysis of GS myoglobin protein levels at the steady state and after ALA treatment. A representative image is shown, with tubulin expression as a loading control. Band intensities were measured by densitometry and normalized to tubulin expression.
(G) Immunofluorescence staining of hypoxic myofibers (green: laminin, hypoxyprobe: red). A representative image is shown, with high magnification in the boxed area.
(H) EM pictures showing enlarged mitochondria with rarefied cristae in 10-month-old *Flvcr1a*^{KO} GS.
(I) EM pictures showing highly electron-dense iron-containing deposits in the mitochondria of Pearls' stained *Flvcr1a*^{KO} GS sections.
(J) Iron quantification in total muscle lysate and in muscle mitochondrial fraction.
(K) Western blot analysis of GS expression of the mitochondrial proteins dynamin-related protein 1 (DRP1), mitofusin 2 (MFN2), peroxisome proliferator-activated receptor-gamma coactivator 1alpha (PGC1a), and translocase of outer mitochondrial membrane 20 (TOM20). A representative image is shown, with vinculin expression as a loading control for all the proteins. Band intensities were measured by densitometry and normalized to vinculin expression.
(L) EM pictures of GS sections, showing the conversion of mitochondrial cristae to electron-dense multilamellar structures in 10-month-old *Flvcr1a*^{KO} GS.
(M) Western blot analysis of LC3-binding chaperone p62 (P62), autophagy related 7 (ATG7), and microtubule-associated protein 1 and 2 light chain 3 (LC3-II/LC3-I) protein levels. A representative image is shown, with vinculin expression as a loading control for all the proteins. Band intensities were measured by densitometry and normalized to vinculin expression.
Scale bar: 200 μm (B, C, E, and G), 50 μm (boxed area in G), and directly indicated on the EM images (H, I, and L). Group averages were compared using the two-way ANOVA test (B and C), the unpaired Student's t test (D, E, J, K, and M), and the one-way ANOVA test (F). *$p < 0.05$, **$p < 0.01$, and ***$p < 0.001$. Data are presented as mean ± SD with n = 3–4 mice/group (B); n = 2–3 mice/group (C and E); n = 4 (D) mice/group; n = 2 mice/group (F); and n = 3 mice/group (J, K, and M). See also Figures S2–S5.

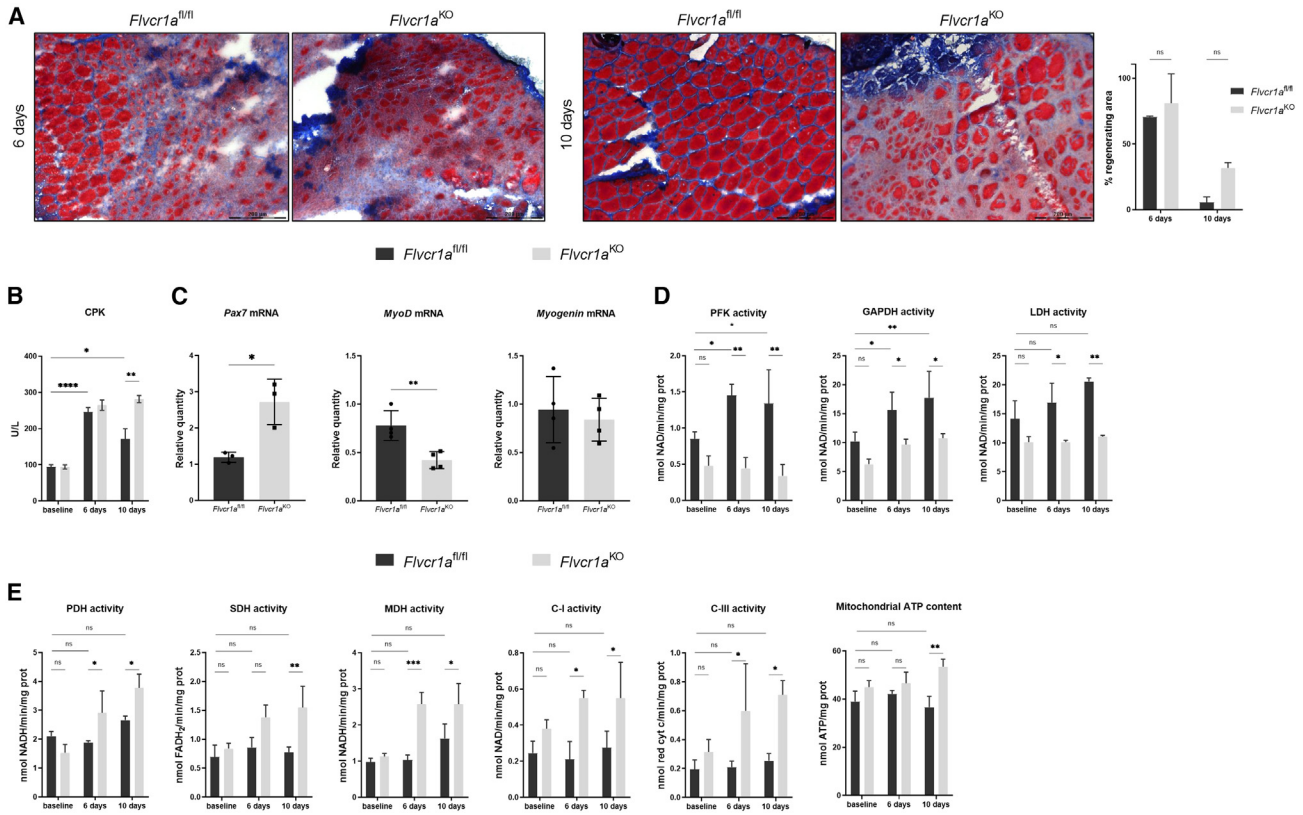

Figure 3. Disrupted heme synthesis-FLVCR1a system results in untimely SC differentiation and compromised muscle regeneration

(A) Representative images of modified Gömöri trichrome staining on TA 6 and 10 days after CTX treatment and quantification of regenerating area.

(B) Serum creatine phosphokinase (CPK) quantification in mice untreated (baseline) or treated with CTX and analyzed 6 or 10 days after.

(C) Real-time RT-qPCR analyses of TA paired box 7 (*Pax7*), myoblast determination protein (*MyoD*), and *myogenin* expression in CTX-treated mice.

(D and E) Activity of some key enzymes involved in glycolysis (D) and oxidative metabolism (E), as well as mitochondrial ATP levels (E), in TA of mice untreated (baseline) or treated with CTX and analyzed 6 or 10 days after. PFK, phosphofructokinase; GAPDH, glyceraldehyde 3-phosphate dehydrogenase; LDH, lactate dehydrogenase; PDH, pyruvate dehydrogenase; SDH, succinate dehydrogenase; MDH, malate dehydrogenase; C-I, complex I; C-III, complex III.

Group averages were compared using two-way ANOVA (A, B, D, and E) and unpaired Student's t test (C). *$p < 0.05$, **$p < 0.01$, ***$p < 0.001$, and ****$p < 0.0001$. Data are presented as mean ± SD with n = 2–3 mice/group (A, D, and E) and n = 3–4 mice/group (B and C).

as we did not observe alterations in vasculature (Figure S5A) and vascular endothelial growth factor A mRNA levels (Figure S5B). Moreover, we observed the induction of erythropoietin expression in the kidneys (Figure S5C), which correlated with elevated levels of red blood cells, hemoglobin, and hematocrit (Figure S5D) in blood analyses, indicating the promotion of erythropoiesis in *Flvcr1a*^{KO} mice, possibly as a compensatory body attempt to counteract the skeletal muscle local hypoxia, albeit unsuccessfully.

Collectively, these data indicate that reduced heme biosynthesis in *Flvcr1a*^{KO} mice affects myoglobin production, likely impairing oxygen management in oxidative muscle fibers.

Flvcr1a loss perturbs mitochondrial integrity

Apart from the deficiency in myoglobin, other factors may contribute to the defective OXPHOS in *Flvcr1a*^{KO} muscle. Indeed, electron microscopy (EM) micrographs revealed the presence of enlarged mitochondria, with rarefied cristae in *Flvcr1a*^{KO} mice (Figure 2H), indicating a profound impairment of mitochondrial integrity.

Perturbed heme metabolism can alter tissue iron stores,[15–17] and reduced heme biosynthesis might conceivably alter tissue iron utilization. Perl's staining on tissue sections for EM revealed highly electron-dense iron-containing deposits in *Flvcr1a*^{KO} mitochondria (Figure 2I). Moreover, while total muscle iron content was unaffected in *Flvcr1a*^{KO} mice, inductively coupled mass spectrometry measurement confirmed increased iron levels in FLVCR1a-deficient mitochondria (Figure 2J). As abnormal iron deposits have been proposed to underpin alterations in mitochondrial dynamics[18,19] and dysfunctional autophagy,[20] we analyzed the expression of proteins involved in these processes. Although the expression of peroxisome proliferator-activated receptor-gamma co-activator 1alpha and of translocase of outer mitochondrial membrane 20, key markers of mitochondrial content, was unchanged in *Flvcr1a*^{KO} mice (Figure 2K), that of dynamin-related protein 1 and mitofusin 2 was significantly reduced (Figure 2K), conceivably suggesting impairment of mitochondrial dynamics. Concomitantly, EM pictures revealed the presence of electron-dense areas in mitochondria, reminiscent of autophagic structures (Figure 2L). In addition, the ratio between

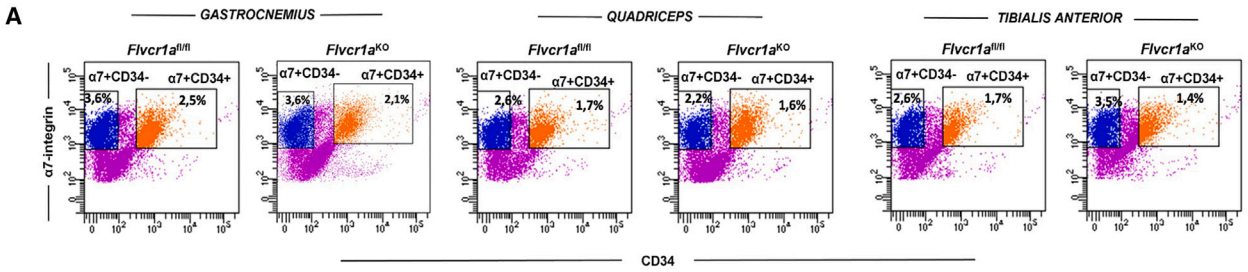

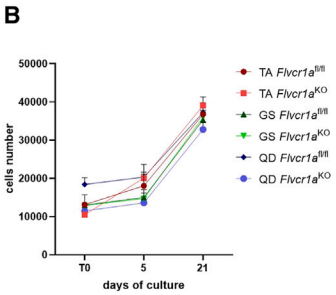

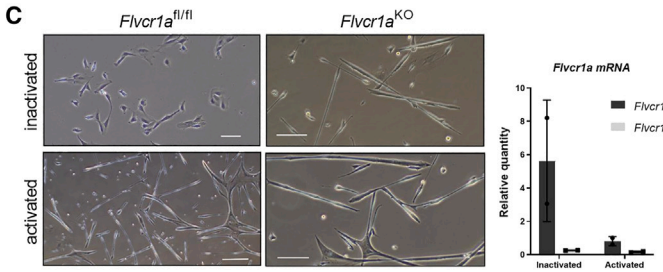

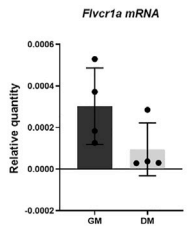

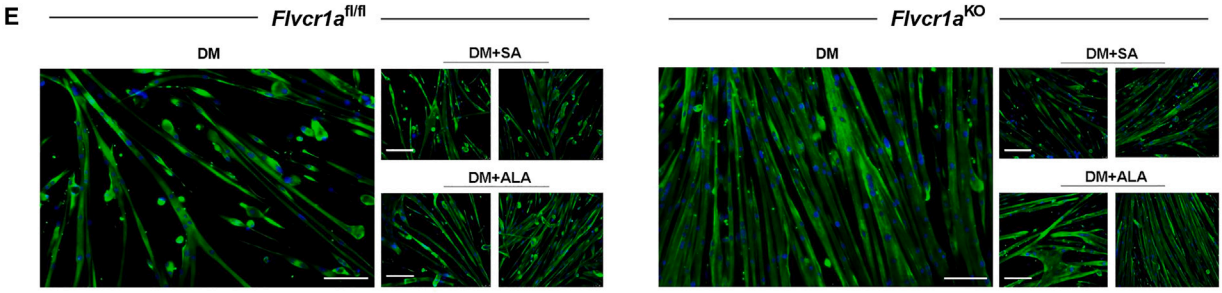

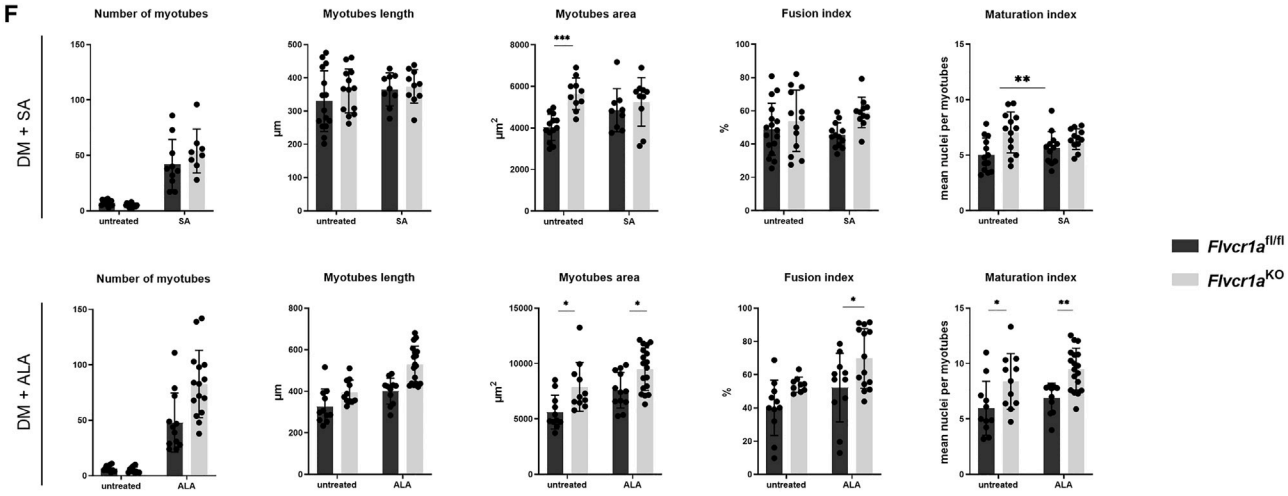

(legend on next page)

microtubule-associated protein 1 and 2 light chain 3 was increased, whereas LC3-binding chaperone p62 and autophagy related 7 protein levels were down-regulated in *Flvcr1a*^{KO} mice compared to controls (Figure 2M), indicating dysfunctional autophagy in *Flvcr1a*^{KO} muscle.

Thus, FLVCR1a loss in skeletal muscle results in mitochondrial damage and reduced oxidative metabolism, likely elicited, at least in part, by myoglobin deficiency, altered mitochondrial dynamics, and dysfunction of the autophagic flux.

Disrupted heme synthesis-FLVCR1a system results in untimely SC differentiation and compromised muscle regeneration

Literature data described a progressive metabolic shift from glycolysis to OXPHOS during activation of muscle stem cells,[12] and in parallel, it has been reported that metabolic pressure contributes to define muscle stem cell fate and activation.[2] To investigate whether the metabolic derangement observed in *Flvcr1a*^{KO} skeletal muscle may impact the SCs' properties and tissue regenerative potential, we injected cardiotoxin (CTX) in *Flvcr1a*^{KO} and *Flvcr1a*$^{fl/fl}$ TA to induce muscle damage. Both control and *Flvcr1a*^{KO} mice showed severe muscle damage 6 days after CTX treatment (Figure 3A), as well as centronucleated myofibers, indicating regeneration, 10 days after CTX injection. However, *Flvcr1a*^{KO} muscles exhibited disorganized muscle structure and infiltration of interstitial cells, indicating a delayed regenerative response (Figure 3A). Moreover, 10 days after the injury, *Flvcr1a*^{KO} muscles showed increased levels of muscle damage markers such as creatine phosphokinase (Figure 3B).[21,22] In addition, the mRNA levels of paired box 7 (a promoter of quiescence) were higher in CTX-injured *Flvcr1a*^{KO} muscles, whereas myoblast determination protein (crucial for specification) was significantly reduced compared to CTX-injured *Flvcr1a*$^{fl/fl}$ TA (Figure 3C). By contrast, myogenin expression (required for differentiation) was comparable in the two genotypes (Figure 3C). Finally, analyses on metabolic pathways revealed that CTX-injured *Flvcr1a*^{KO} TAs were unable to increase glycolysis during regeneration, as CTX-injured *Flvcr1a*$^{fl/fl}$ muscles did, with a consequent precocious shift toward oxidative metabolism (Figures 3D and 3E). Taken together, these findings point to impaired engagement of metabolic processes during muscle regeneration in *Flvcr1a*^{KO} mice, thus putting forward the notion that CTX-injured *Flvcr1a*^{KO} muscles prematurely activate SC differentiation, with a consequent delayed regenerative process.

We then investigated the impact of FLVCR1a on myogenic fate decisions in SCs isolated from muscles. Quiescent inactivated (α7-integrin+CD34^{+}) and activated (α7-integrin+CD34^{-}) *Flvcr1a*^{KO} and *Flvcr1a*$^{fl/fl}$ SCs were represented in similar proportions (Figure 4A) and showed similar proliferation rates when plated in growth medium (GM) (Figure 4B). Interestingly, both inactivated and activated *Flvcr1a*^{KO} SCs spontaneously form larger myotubes in GM, suggesting a premature progression to myogenic lineage (Figure 4C). Moreover, *Flvcr1a* mRNA was significantly reduced in activated compared to inactivated *Flvcr1a*$^{fl/fl}$ SCs (Figure 4C). Similarly, we detected a decrease in *Flvcr1a* expression when comparing C2C12 myogenic cells cultured in GM and differentiation medium (Figure 4D), hinting at FLVCR1a involvement in the control of cellular commitment. Likewise, a dramatically lower proportion of desmin+ myotubes was found in *Flvcr1a*^{KO} SCs at day 5 after differentiation (Figure 4E), although their terminal myogenic differentiation was confirmed by higher myotube area and maturation index relative to *Flvcr1a*$^{fl/fl}$ SCs (Figure 4F), further indicating that loss of FLVCR1a results in untimely myogenic differentiation. Taken together, these results suggest that FLVCR1a in SCs is essential for skeletal muscle regeneration and for preventing premature progression to the myogenic lineage, likely by averting an early transition from glycolysis to OXPHOS.

The involvement of the heme synthesis-FLVCR1a axis in the maintenance of cell proliferation[8,9] has been previously described. Moreover, heme biosynthesis has been implicated in the naive-to-primed embryonic stem cell transition,[23–25] a shift from two different pluripotent states exhibiting contrasting metabolic requirements.[26] Therefore, we hypothesize that dysregulated heme biosynthesis could be the underlying cause of premature myogenic differentiation in *Flvcr1a*^{KO} SCs. As previously explained, ALAS1 concomitantly plays a role in heme production and contributes to TCA cycle cataplerosis. This means that ALAS1 activity can impact cellular metabolism both dependently on and independently of heme. Consequently, to test the implication of heme biosynthesis in SC differentiation, we harnessed two distinct compounds: ALA and succinyl-acetone (SA). ALA, as mentioned previously, induces *de novo* heme biosynthesis, bypassing ALAS1. Therefore, it increases heme levels but concomitantly reduces ALAS1 activity,[9] as ALAS1 is feedback inhibited by heme itself. Conversely, SA inhibits the second heme biosynthetic enzyme, thus decreasing heme levels while concurrently promoting ALAS1 activity,[27,28] as feedback inhibition is released. Consequently, the administration of ALA and SA to *Flvcr1a*^{KO} and *Flvcr1a*$^{fl/fl}$ SCs, along with their comparison, enabled us to dissect the effects stemming from heme levels from those associated with ALAS1 activity per se.

Figure 4. Disrupted heme synthesis-FLVCR1a system results in untimely SC differentiation

(A) Fluorescence-activated cell sorting (FACS) analysis dot plots showing the different GS, TA, and QD SC subpopulations in 10-month-old mice.

(B) Proliferation assays of SCs isolated from 10-month-old TA, GS, and QD.

(C) Representative images of inactivated and activated cultured SCs isolated from 5-month-old skeletal muscle and real-time RT-qPCR analysis of their *Flvcr1a* mRNA levels.

(D) Real-time RT-qPCR analysis of *Flvcr1a* expression in C2C12 cells before (growth medium [GM]) and after (differentiating medium [DM]) differentiation.

(E) Immunofluorescence staining (blue: DAPI, red: desmin) of SCs isolated from 5-month-old skeletal muscle and cultured for 7 days in DM in the absence of any treatment (DM), in DM supplemented with 5 mM ALA (DM + ALA), or in DM supplemented with 0.5 mM SA (DM + SA). Representative images are shown.

(F) Measurements of some key parameters for myotube number, morphology, and differentiation in SCs isolated from 5-month-old skeletal muscle cultured in DM, DM + ALA, and DM + SA.

Scale bar: 50 μm (C and E). Group averages were compared using two-way ANOVA. *$p < 0.05$, **$p < 0.01$, and ***$p < 0.001$. Data are presented as mean ± SD with n = 8 (A); n = 6 per group (B and C); n = 4 (D); and n = 12 (E and F).

We observed that SA treatment in *Flvcr1a*^{KO} SCs effectively restored the number of myotubes, which displayed a similar proportion of myotube area and maturation index compared to *Flvcr1a*$^{fl/fl}$ SCs (Figures 4E and 4F), underscoring the normalization of premature progression to the myogenic lineage in differentiating SA-treated *Flvcr1a*^{KO} SCs. In contrast, ALA treatment in *Flvcr1a*$^{fl/fl}$ SCs mimicked the effects of *Flvcr1a* deletion. Moreover, ALA administration exacerbated the existing differences observed in *Flvcr1a*^{KO} and *Flvcr1a*$^{fl/fl}$ SCs at day 7 after differentiation (Figures 4E and 4F).

Although ALAS1 activity is not entirely distinct from heme production, these findings suggest that diminished ALAS1 activity, rather than heme levels, primarily triggers premature differentiation in *Flvcr1a*^{KO} SCs.

DISCUSSION

The present work elucidates the importance of FLVCR1a in the control of the acquisition/maintenance of a specific energy profile in muscle progenitors and fibers.

FLVCR1a's role is debated: it may export heme[3] or import choline.[4–7] However, *Flvcr1a* loss reduces heme biosynthesis, regardless of its cargo. ALAS1-mediated heme biosynthesis influences mitochondrial oxidative metabolism, both supporting it, by supplying the heme co-factor to the ETC complexes,[29] and hindering it, by consuming succinyl-CoA, functioning as a TCA cycle cataplerotic pathway.[8] FLVCR1a has been described as a partner of ALAS1,[8,9,14] capable of determining its activity. Therefore, our data sustain a model in which FLVCR1a promotes heme synthesis in skeletal muscle cells, both favoring the production of myoglobin and balancing the pro-oxidative *vs.* the pro-glycolytic function of heme biosynthesis, thus contributing to determine their energy phenotype. As a consequence, the disruption of the heme synthesis-FLVCR1a system leads to dysregulated fiber metabolism, with muscle cells primed to be oxidative but unable to execute proper OXPHOS.

Our data show a clear link between reduced ALAS1-dependent heme biosynthesis and metabolic changes in *Flvcr1a*^{KO} muscles and differentiating SCs. Indeed, treating SCs with agents affecting heme biosynthesis mirrors/reverses the abnormal myogenic commitment seen in *Flvcr1a*^{KO} SCs. Previous works elucidated the importance of heme biosynthesis in the transition of pluripotent cells between different states.[23–25] Moreover, the involvement of heme metabolism in SC differentiation is in line with studies reporting HO-1 as a regulator of differentiation of muscle progenitors *in vitro*.[30,31] Furthermore, similar to the muscle-specific *Flvcr1a*-null mice, skeletal-muscle-specific HO-1-null (MHO1) animals show compromised muscle integrity and performance, characterized by muscle fiber atrophy, mitochondrial damage, reduced oxidative metabolism, and deregulated muscle cell differentiation, suggesting the presence of a shared fundamental dysfunction in the two mouse models. Nevertheless, unlike prior studies, our data propose a different perspective, suggesting that FLVCR1a serves as a precise mechanism for regulating ALAS1 activity and heme synthesis for energetic purposes, likely ensuring that cells acquire the proper energetic phenotype for transitioning among a quiescent-proliferative-differentiated state. Consistent with our observations in *Flvcr1a*^{KO} SCs, previous studies reported FLVCR1a expression modulation during erythroid and endothelial cell differentiation,.[32,33] Likewise, defective expansion and differentiation of erythroid progenitors[34] and impaired regeneration of intestinal mucosa upon injury[16] have already been described in animal models tissue-specifically null for FLVCR1a.

The reasons for ETC impairment in MHO1 mice, with heme accumulation, and muscle-specific *Flvcr1a*^{KO} mice, with reduced heme synthesis, are not fully understood. Heme toxicity could distress mitochondria in MHO1 mice, while reduced *de novo* heme supply by ALAS1 might decrease ETC in *Flvcr1a*^{KO} mice. However, based on data obtained in other systems,[8] this alone may not fully explain ETC malfunction in *Flvcr1a*^{KO} mice. Secondary factors, like impaired mitochondrial morphology/dynamics,[35] altered autophagy,[36] and decreased myoglobin production could also contribute.

In conclusion, the heme synthesis-FLVCR1a system controls muscle energy phenotype, thereby suggesting potential avenues for modulating skeletal muscle function and stem cell state by targeting metabolic pathways controlled by/interlinked with ALAS1-mediated heme biosynthesis.

Limitations of the study

Our study did not examine heme dynamics with the required accuracy, so it does not conclusively determine if FLVCR1a transports both heme and choline or if one affects the other's transport. Thus, how FLVCR1a regulates ALAS1 activity remains uncertain. Further research is needed to clarify the molecular pathways linking heme and choline metabolism.

STAR★METHODS

Detailed methods are provided in the online version of this paper and include the following:

- KEY RESOURCES TABLE
- RESOURCE AVAILABILITY
  - Lead contact
  - Materials availability
  - Data and code availability
- EXPERIMENTAL MODEL AND SUBJECT PARTICIPANT DETAILS
  - Primary cell cultures
  - Cell lines
  - Animal models
- METHOD DETAILS
  - RNA extraction and quantitative real-time PCR
  - Protein extraction and western blot
  - Mitochondria isolation for enzymatic assays
  - Mitochondrial ATP content
  - Enzymatic activity
  - Histological and immunofluorescence analysis
  - Muscle hypoxia
  - Grip strength test
  - Kondziela's inverted screen test
  - Rotarod performance test
  - Treadmill performance test
  - Electron microscopy

- Tissue iron content measurement by ICP-MS
- Tissue heme content measurement
- Tissue free choline content measurement
- Cardiotoxin treatment
- Blood and serum analysis
- ALA and SA satellite cells treatment

- QUANTIFICATION AND STATISTICAL ANALYSIS

SUPPLEMENTAL INFORMATION

Supplemental information can be found online at https://doi.org/10.1016/j.celrep.2024.113854.

ACKNOWLEDGMENTS

The authors are grateful to Prof. Giorgio Roberto Merlo for helpful discussion and Dr. Silene Giusti for help with some experiments. This work was supported by the Italian Regenerative Medicine Infrastructure (IRMI) grant CTN01_00177_888744 and the Progetti di Rilevanza e Interesse Nazionale (PRIN 2022) grant 2022XJNWRM to E. Tolosano, and Y.T. is the recipient of Unmet Medical Needs, Fondazione Regionale per la Ricerca Biomedica (FRRB-2022; Project REMODEL, PR-0490, CDC/CDR 230R16); Gruppo Familiari Beta-Sarcoglicanopatie (GFB-ONLUS, Project PR-0394); Piano Nazionale di Ripresa e Resilienza (PNRR) National Center for Gene Therapy and Drugs based on RNA Technology (PNRR CN3 RNA, 2022; Spoke #1: Genetic diseases), NextGenerationEU, MUR; and Cariplo Telethon Alliance GJC2021 (project #GJC21084). Figures 2A and S1A and the graphical abstract were created with BioRender (https://www.biorender.com).

AUTHOR CONTRIBUTIONS

Conceptualization and visualization, M. Mistretta, V.F., E. Tolosano, and Y.T.; methodology, E. Tolosano, Y.T., and P.E.P.; formal analysis, M. Mistretta, V.F., and C.R.; investigation, M. Mistretta, V.F., A.L.A., G.A., M.H., S.D., M.B., L.N., M.R., E. Trombetta, P.M., A.F., M. Meregalli, C.V., B.M., S.G.C., and C.R.; writing – original draft, M. Mistretta and V.F.; writing – review & editing, M. Mistretta, V.F., E. Tolosano, and Y.T.; supervision, project administration, and funding acquisition, E. Tolosano and Y.T.

DECLARATION OF INTERESTS

The authors declare no competing interests.

DECLARATION OF GENERATIVE AI AND AI-ASSISTED TECHNOLOGIES IN THE WRITING PROCESS

During the preparation of this work, the authors used the ChatGPT AI system in order to improve language and readability. After using this tool/service, the authors reviewed and edited the content as needed and take full responsibility for the content of the publication.

Received: June 30, 2023
Revised: December 7, 2023
Accepted: February 8, 2024
Published: February 26, 2024

REFERENCES

1. MAURO, A. (1961). Satellite cell of skeletal muscle fibers. J. Biophys. Biochem. Cytol. *9*, 493–495. https://doi.org/10.1083/jcb.9.2.493.
2. Abreu, P. (2018). Bioenergetics mechanisms regulating muscle stem cell self-renewal commitment and function. Biomed. Pharmacother. *103*, 463–472. https://doi.org/10.1016/j.biopha.2018.04.036.
3. Quigley, J.G., Yang, Z., Worthington, M.T., Phillips, J.D., Sabo, K.M., Sabath, D.E., Berg, C.L., Sassa, S., Wood, B.L., and Abkowitz, J.L. (2004). Identification of a human heme exporter that is essential for erythropoiesis. Cell *118*, 757–766. https://doi.org/10.1016/j.cell.2004.08.014.
4. Moore, A., Busch, M.P., Dziewulska, K., Francis, R.O., Hod, E.A., Zimring, J.C., D'Alessandro, A., and Page, G.P. (2022). Genome-wide metabolite quantitative trait loci analysis (mQTL) in red blood cells from volunteer blood donors. J. Biol. Chem. *298*, 102706. https://doi.org/10.1016/j.jbc.2022.102706.
5. Tsuchiya, M., Tachibana, N., Nagao, K., Tamura, T., and Hamachi, I. (2023). Organelle-selective click labeling coupled with flow cytometry allows pooled CRISPR screening of genes involved in phosphatidylcholine metabolism. Cell Metab. *35*, 1072–1083.e9. https://doi.org/10.1016/j.cmet.2023.02.014.
6. Kenny, T.C., Khan, A., Son, Y., Yue, L., Heissel, S., Sharma, A., Pasolli, H.A., Liu, Y., Gamazon, E.R., Alwaseem, H., et al. (2023). Integrative genetic analysis identifies FLVCR1 as a plasma-membrane choline transporter in mammals. Cell Metab. *35*, 1057–1071.e12. https://doi.org/10.1016/j.cmet.2023.04.003.
7. Ha, H.T.T., Sukumar, V.K., Chua, J.W.B., Nguyen, D.T., Nguyen, T.Q., Lim, L.H.K., Cazenave-Gassiot, A., and Nguyen, L.N. (2023). Mfsd7b facilitates choline transport and missense mutations affect choline transport function. Cell. Mol. Life Sci. *81*, 3. https://doi.org/10.1007/s00018-023-05048-4.
8. Fiorito, V., Allocco, A.L., Petrillo, S., Gazzano, E., Torretta, S., Marchi, S., Destefanis, F., Pacelli, C., Audrito, V., Provero, P., et al. (2021). The heme synthesis-export system regulates the tricarboxylic acid cycle flux and oxidative phosphorylation. Cell Rep. *35*, 109252. https://doi.org/10.1016/j.celrep.2021.109252.
9. Allocco, A.L., Bertino, F., Petrillo, S., Chiabrando, D., Riganti, C., Bardelli, A., Altruda, F., Fiorito, V., and Tolosano, E. (2022). Inhibition of Heme Export and/or Heme Synthesis Potentiates Metformin Anti-Proliferative Effect on Cancer Cell Lines. Cancers *14*, 1230.
10. Petrillo, S., Chiabrando, D., Genova, T., Fiorito, V., Ingoglia, G., Vinchi, F., Mussano, F., Carossa, S., Silengo, L., Altruda, F., et al. (2018). Heme accumulation in endothelial cells impairs angiogenesis by triggering paraptosis. Cell Death Differ. *25*, 573–588. https://doi.org/10.1038/s41418-017-0001-7.
11. Taylor, S.C., Berkelman, T., Yadav, G., and Hammond, M. (2013). A defined methodology for reliable quantification of Western blot data. Mol. Biotechnol. *55*, 217–226. https://doi.org/10.1007/s12033-013-9672-6.
12. Relaix, F., Bencze, M., Borok, M.J., Der Vartanian, A., Gattazzo, F., Mademtzoglou, D., Perez-Diaz, S., Prola, A., Reyes-Fernandez, P.C., Rotini, A., and Taglietti. (2021). Perspectives on skeletal muscle stem cells. Nat. Commun. *12*, 692. https://doi.org/10.1038/s41467-020-20760-6.
13. Bhattacharya, D., and Scimè, A. (2020). Mitochondrial Function in Muscle Stem Cell Fates. Front. Cell Dev. Biol. *8*, 480. https://doi.org/10.3389/fcell.2020.00480.
14. Vinchi, F., Ingoglia, G., Chiabrando, D., Mercurio, S., Turco, E., Silengo, L., Altruda, F., and Tolosano, E. (2014). Heme exporter FLVCR1a regulates heme synthesis and degradation and controls activity of cytochromes P450. Gastroenterology *146*, 1325–1338. https://doi.org/10.1053/j.gastro.2014.01.053.
15. Fiorito, V., Geninatti Crich, S., Silengo, L., Aime, S., Altruda, F., and Tolosano, E. (2013). Lack of Plasma Protein Hemopexin Results in Increased Duodenal Iron Uptake. PLoS One *8*, e68146. https://doi.org/10.1371/journal.pone.0068146.
16. Fiorito, V., Forni, M., Silengo, L., Altruda, F., and Tolosano, E. (2015). Crucial Role of FLVCR1a in the Maintenance of Intestinal Heme Homeostasis. Antioxid. Redox Signal. *23*, 1410–1423. https://doi.org/10.1089/ars.2014.6216.
17. Morello, N., Tonoli, E., Logrand, F., Fiorito, V., Fagoonee, S., Turco, E., Silengo, L., Vercelli, A., Altruda, F., and Tolosano, E. (2009). Haemopexin affects iron distribution and ferritin expression in mouse brain. J. Cell Mol. Med. *13*, 4192–4204. https://doi.org/10.1111/j.1582-4934.2008.00611.x.

18. Zheng, Q., Zhao, Y., Guo, J., Zhao, S., Fei, C., Xiao, C., Wu, D., Wu, L., Li, X., and Chang, C. (2018). Iron overload promotes mitochondrial fragmentation in mesenchymal stromal cells from myelodysplastic syndrome patients through activation of the AMPK/MFF/Drp1 pathway. Cell Death Dis. *9*, 515. https://doi.org/10.1038/s41419-018-0552-7.

19. Sumneang, N., Siri-Angkul, N., Kumfu, S., Chattipakorn, S.C., and Chattipakorn, N. (2020). The effects of iron overload on mitochondrial function, mitochondrial dynamics, and ferroptosis in cardiomyocytes. Arch. Biochem. Biophys. *680*, 108241. https://doi.org/10.1016/j.abb.2019.108241.

20. Wang, Y., Wang, M., Liu, Y., Tao, H., Banerjee, S., Srinivasan, S., Nemeth, E., Czaja, M.J., and He, P. (2022). Integrated regulation of stress responses, autophagy and survival by altered intracellular iron stores. Redox Biol. *55*, 102407. https://doi.org/10.1016/j.redox.2022.102407.

21. Pettersson, J., Hindorf, U., Persson, P., Bengtsson, T., Malmqvist, U., Werkström, V., and Ekelund, M. (2008). Muscular exercise can cause highly pathological liver function tests in healthy men. Br. J. Clin. Pharmacol. *65*, 253–259. https://doi.org/10.1111/j.1365-2125.2007.03001.x.

22. Hazar, M., Otag, A., Otag, I., Sezen, M., and Sever, O. (2014). Effect of increasing maximal aerobic exercise on serum muscles enzymes in professional field hockey players. Glob. J. Health Sci. *7*, 69–74. https://doi.org/10.5539/gjhs.v7n3p69.

23. Mathieu, J., Detraux, D., Kuppers, D., Wang, Y., Cavanaugh, C., Sidhu, S., Levy, S., Robitaille, A.M., Ferreccio, A., Bottorff, T., et al. (2019). Folliculin regulates mTORC1/2 and WNT pathways in early human pluripotency. Nat. Commun. *10*, 632. https://doi.org/10.1038/s41467-018-08020-0.

24. Li, M., Yu, J.S.L., Tilgner, K., Ong, S.H., Koike-Yusa, H., and Yusa, K. (2018). Genome-wide CRISPR-KO Screen Uncovers mTORC1-Mediated Gsk3 Regulation in Naive Pluripotency Maintenance and Dissolution. Cell Rep. *24*, 489–502. https://doi.org/10.1016/j.celrep.2018.06.027.

25. Detraux, D., Caruso, M., Feller, L., Fransolet, M., Meurant, S., Mathieu, J., Arnould, T., and Renard, P. (2023). A critical role for heme synthesis and succinate in the regulation of pluripotent states transitions. Elife *12*, e78546. https://doi.org/10.7554/eLife.78546.

26. Zhou, W., Choi, M., Margineantu, D., Margaretha, L., Hesson, J., Cavanaugh, C., Blau, C.A., Horwitz, M.S., Hockenbery, D., Ware, C., and Ruohola-Baker, H. (2012). HIF1α induced switch from bivalent to exclusively glycolytic metabolism during ESC-to-EpiSC/hESC transition. EMBO J. *31*, 2103–2116. https://doi.org/10.1038/emboj.2012.71.

27. Chernova, T., Steinert, J.R., Guerin, C.J., Nicotera, P., Forsythe, I.D., and Smith, A.G. (2007). Neurite degeneration induced by heme deficiency mediated via inhibition of NMDA receptor-dependent extracellular signal-regulated kinase 1/2 activation. J. Neurosci. *27*, 8475–8485. https://doi.org/10.1523/JNEUROSCI.0792-07.2007.

28. De Matteis, F., and Ray, D.E. (1982). Studied on cerebellar haem metabolism in the rat in vivo. J. Neurochem. *39*, 551–556. https://doi.org/10.1111/j.1471-4159.1982.tb03980.x.

29. Kim, H.J., Khalimonchuk, O., Smith, P.M., and Winge, D.R. (2012). Structure, function, and assembly of heme centers in mitochondrial respiratory complexes. Biochim. Biophys. Acta *1823*, 1604–1616. https://doi.org/10.1016/j.bbamcr.2012.04.008.

30. Pilegaard, H., Ordway, G.A., Saltin, B., and Neufer, P.D. (2000). Transcriptional regulation of gene expression in human skeletal muscle during recovery from exercise. Am. J. Physiol. Endocrinol. Metab. *279*, E806–E814. https://doi.org/10.1152/ajpendo.2000.279.4.E806.

31. Ren, C., Qi, J., Li, W., and Zhang, J. (2016). The effect of moderate-intensity exercise on the expression of HO-1 mRNA and activity of HO in cardiac and vascular smooth muscle of spontaneously hypertensive rats. Can. J. Physiol. Pharmacol. *94*, 448–454. https://doi.org/10.1139/cjpp-2015-0122.

32. Doty, R.T., Phelps, S.R., Shadle, C., Sanchez-Bonilla, M., Keel, S.B., and Abkowitz, J.L. (2015). Coordinate expression of heme and globin is essential for effective erythropoiesis. J. Clin. Invest. *125*, 4681–4691. https://doi.org/10.1172/JCI83054.

33. Petrillo, S., De Giorgio, F., Bertino, F., Garello, F., Bitonto, V., Longo, D.L., Mercurio, S., Ammirata, G., Allocco, A.L., Fiorito, V., et al. (2023). Endothelial cells require functional FLVCR1a during developmental and adult angiogenesis. Angiogenesis *26*, 365–384. https://doi.org/10.1007/s10456-023-09865-w.

34. Mercurio, S., Petrillo, S., Chiabrando, D., Bassi, Z.I., Gays, D., Camporeale, A., Vacaru, A., Miniscalco, B., Valperga, G., Silengo, L., et al. (2015). The heme exporter Flvcr1 regulates expansion and differentiation of committed erythroid progenitors by controlling intracellular heme accumulation. Haematologica *100*, 720–729. https://doi.org/10.3324/haematol.2014.114488.

35. Liesa, M., and Shirihai, O.S. (2013). Mitochondrial dynamics in the regulation of nutrient utilization and energy expenditure. Cell Metab. *17*, 491–506. https://doi.org/10.1016/j.cmet.2013.03.002.

36. Bosc, C., Broin, N., Fanjul, M., Saland, E., Farge, T., Courdy, C., Batut, A., Masoud, R., Larrue, C., Skuli, S., et al. (2020). Autophagy regulates fatty acid availability for oxidative phosphorylation through mitochondria-endoplasmic reticulum contact sites. Nat. Commun. *11*, 4056. https://doi.org/10.1038/s41467-020-17882-2.

37. Kanisicak, O., Mendez, J.J., Yamamoto, S., Yamamoto, M., and Goldhamer, D.J. (2009). Progenitors of skeletal muscle satellite cells express the muscle determination gene, MyoD. Dev. Biol. *332*, 131–141. https://doi.org/10.1016/j.ydbio.2009.05.554.

38. Schindelin, J., Arganda-Carreras, I., Frise, E., Kaynig, V., Longair, M., Pietzsch, T., Preibisch, S., Rueden, C., Saalfeld, S., Schmid, B., et al. (2012). Fiji: an open-source platform for biological-image analysis. Nat. Methods *9*, 676–682. https://doi.org/10.1038/nmeth.2019.

39. Florio, F., Accordini, S., Libergoli, M., and Biressi, S. (2022). Targeting Muscle-Resident Single Cells Through. Front. Physiol. *13*, 834705. https://doi.org/10.3389/fphys.2022.834705.

40. Chen, J.C.J., Mortimer, J., Marley, J., and Goldhamer, D.J. (2005). MyoD-cre transgenic mice: a model for conditional mutagenesis and lineage tracing of skeletal muscle. Genesis *41*, 116–121. https://doi.org/10.1002/gene.20104.

41. Destefanis, F., Fiorito, V., Altruda, F., and Tolosano, E. (2019). Investigating the Connection Between Endogenous Heme Accumulation and COX2 Activity in Cancer Cells. Front. Oncol. *9*, 162. https://doi.org/10.3389/fonc.2019.00162.

42. Wibom, R., Hagenfeldt, L., and von Döbeln, U. (2002). Measurement of ATP production and respiratory chain enzyme activities in mitochondria isolated from small muscle biopsy samples. Anal. Biochem. *311*, 139–151.

43. Bergonia, H.A., Franklin, M.R., Kushner, J.P., and Phillips, J.D. (2015). A method for determining δ-aminolevulinic acid synthase activity in homogenized cells and tissues. Clin. Biochem. *48*, 788–795. https://doi.org/10.1016/j.clinbiochem.2015.04.023.

44. Sharma, B. (2011). Kinetic Characterisation of Phosphofructokinase Purified from Setaria cervi: A Bovine Filarial Parasite. Enzyme Res. *2011*, 939472. https://doi.org/10.4061/2011/939472.

45. Riganti, C., Aldieri, E., Bergandi, L., Fenoglio, I., Costamagna, C., Fubini, B., Bosia, A., and Ghigo, D. (2002). Crocidolite asbestos inhibits pentose phosphate oxidative pathway and glucose 6-phosphate dehydrogenase activity in human lung epithelial cells. Free Radic. Biol. Med. *32*, 938–949. https://doi.org/10.1016/s0891-5849(02)00800-6.

46. Capello, M., Ferri-Borgogno, S., Riganti, C., Chattaragada, M.S., Principe, M., Roux, C., Zhou, W., Petricoin, E.F., Cappello, P., and Novelli, F. (2016). Targeting the Warburg effect in cancer cells through ENO1 knockdown rescues oxidative phosphorylation and induces growth arrest. Oncotarget *7*, 5598–5612. https://doi.org/10.18632/oncotarget.6798.

47. Drouin, G., Couture, V., Lauzon, M.A., Balg, F., Faucheux, N., and Grenier, G. (2019). Muscle injury-induced hypoxia alters the proliferation and differentiation potentials of muscle resident stromal cells. Skelet. Muscle *9*, 18. https://doi.org/10.1186/s13395-019-0202-5.

48. Deacon, R.M. (2013). Measuring the strength of mice. J. Vis. Exp. *76*, 2610. https://doi.org/10.3791/2610.

49. Morello, N., Bianchi, F.T., Marmiroli, P., Tonoli, E., Rodriguez Menendez, V., Silengo, L., Cavaletti, G., Vercelli, A., Altruda, F., and Tolosano, E. (2011). A role for hemopexin in oligodendrocyte differentiation and myelin formation. PLoS One *6*, e20173. https://doi.org/10.1371/journal.pone.0020173.

50. Knab, A.M., Bowen, R.S., Moore-Harrison, T., Hamilton, A.T., Turner, M.J., and Lightfoot, J.T. (2009). Repeatability of exercise behaviors in mice. Physiol. Behav. *98*, 433–440. https://doi.org/10.1016/j.physbeh.2009.07.006.

51. Lightfoot, J.T., Turner, M.J., Debate, K.A., and Kleeberger, S.R. (2001). Interstrain variation in murine aerobic capacity. Med. Sci. Sports Exerc. *33*, 2053–2057. https://doi.org/10.1097/00005768-200112000-00012.

52. Lovatel, G.A., Elsner, V.R., Bertoldi, K., Vanzella, C., Moysés, F.D.S., Vizuete, A., Spindler, C., Cechinel, L.R., Netto, C.A., Muotri, A.R., and Siqueira, I.R. (2013). Treadmill exercise induces age-related changes in aversive memory, neuroinflammatory and epigenetic processes in the rat hippocampus. Neurobiol. Learn. Mem. *101*, 94–102. https://doi.org/10.1016/j.nlm.2013.01.007.

53. Sinclair, P.R., Gorman, N., and Jacobs, J.M. (2001). Measurement of heme concentration. Curr Protoc Toxicol *Chapter 8*, tx0803s00, Unit 8.3. https://doi.org/10.1002/0471140856.

54. Maio, N., Singh, A., Uhrigshardt, H., Saxena, N., Tong, W.H., and Rouault, T.A. (2014). Cochaperone binding to LYR motifs confers specificity of iron sulfur cluster delivery. Cell Metab. *19*, 445–457. https://doi.org/10.1016/j.cmet.2014.01.015.

55. Aoki, Y., Nagata, T., Yokota, T., Nakamura, A., Wood, M.J.A., Partridge, T., and Takeda, S. (2013). Highly efficient in vivo delivery of PMO into regenerating myotubes and rescue in laminin-α2 chain-null congenital muscular dystrophy mice. Hum. Mol. Genet. *22*, 4914–4928. https://doi.org/10.1093/hmg/ddt341.

STAR★METHODS

KEY RESOURCES TABLE

REAGENT or RESOURCE	SOURCE	IDENTIFIER
Antibodies		
Mouse monoclonal, Anti-Vinculin	Sigma Aldrich St. Louis, MO, USA	Cat#SAB4200080; RRID: AB_10604160
Anti-7-Amino-Actinomycin D (7-AAD)	BD Biosciences, Franklin Lakes, NJ, USA	Cat#559925; RRID:AB_2869266
Mouse monoclonal, Anti-Atg7	Sigma-Aldrich, St. Louis, MO, USA	Cat#SAB4200304; RRID:AB_10895884
Rat monoclonal, Anti-mouse CD31	BD Biosciences, Franklin Lakes, NJ, USA	Cat#550274; RRID:AB_393571
Rat monoclonal, anti-mouse CD31 FITC conjugated	BD Biosciences, Franklin Lakes, NJ, USA	Cat#558738; RRID:AB_397097
Rat monoclonal, anti-mouse CD45 FITC conjugated	BD Biosciences, Franklin Lakes, NJ, USA	Cat#553080; RRID:AB_394610
Rabbit monoclonal, Anti-DRP1	Abcam, Cambridge, UK	Cat#ab184247; RRID:AB_2895215
Rat monoclonal, anti-mouse F4/80 PE	BD Biosciences, Franklin Lakes, NJ, USA	Cat#565410; RRID:AB_2687527
Rabbit polyclonal, Anti-FLVCR1a	Proteintech, Rosemont, IL, USA	Cat#26841-1-AP; RRID:AB_2880654
Isolectin	Thermofisher Scientific, Waltham, MA, USA	Cat# I21413; RRID: N/A
Rabbit polyclonal, Anti-mouse Laminin	Sigma-Aldrich, St. Louis, MO, USA	Cat#L9393; RRID:AB_477163
Rabbit polyclonal, Anti-LC3B	Sigma-Aldrich, St. Louis, MO, USA	Cat#L7543; RRID: N/A
Rabbit monoclonal, Anti-Mitofusin 2	Cell Signaling Technology, Danvers, MA, USA	Cat#9482S; RRID: N/A
Rabbit monoclonal, Anti-Myoglobin	Abcam, Cambridge, UK	Cat#ab77232; RRID:AB_1523998
Mouse monoclonal, Myosin heavy chain type I antibody	DSHB, Iowa City, Iowa, IA, USA	Cat#BA-d5; RRID:AB_2235587
Mouse monoclonal, Myosin heavy chain type IIA antibody	DSHB, Iowa City, Iowa, IA, USA	Cat#sc-71; RRID:AB_2147165
Mouse monoclonal, Myosin heavy chain type IIB antibody	DSHB, Iowa City, Iowa, IA, USA	Cat#BF-f3; RRID:AB_2266724
Mouse monoclonal, Total OXPHOS Rodent WB Antibody Cocktail	Abcam, Cambridge, UK	Cat#ab110413; RRID:AB_2629281
Rabbit polyclonal, Anti-p62	Sigma-Aldrich, St. Louis, MO, USA	Cat#P0067; RRID:AB_1841064
Mouse monoclonal, Anti-PGC1α	Santa Cruz Biotechnology, Dallas, TX, USA	Cat#sc-518038; RRID:AB_2895142
Rat monoclonal, anti-mouse Sca-1	Miltenyi Biotec, Bergisch Gladbach, DE	Cat#130-126-949; RRID:AB_2905381
Rabbit monoclonal, Anti-TOMM20	Abcam, Cambridge, UK	Cat#ab186735; RRID:AB_2889972
Rabbit polyclonal, anti-HO-1	Enzo Life Sciences, Farmingdale, NY, USA	Cat#ADI-SPA-896-F; RRID:AB_11180765
Chemicals, peptides, and recombinant proteins		
3,3′-diaminobenzidina (DAB)	Sigma Aldrich, St. Louis, MO, USA	Cat#D5905
5-Aminolevulinic acid hydrochloride	Sigma Aldrich, St. Louis, MO, USA	Cat#A3785
Aniline blue	Bio Optica, Milan, IT	Cat#05-B10006
Bouin solution	Chem-lab NV, Zedelgem, BE	Cat#CL04.0204.1000
Cardiotoxin	Latoxan Laboratory, Portes-lès-Valence, FR	Cat#L8102
Chicken Embryo Extract	MP Biomedicals, Irvine, CA, USA	Cat#092850145
Collagenase, Type II	Thermofisher Scientific, Waltham, MA, USA	Cat#17101015
Cytochrome *c*	Sigma Aldrich, St. Louis, MO, USA	Cat#C7752
DPX mountant	VWR International, Radnor, PA, USA	Cat#100504-938
Dispase II	Thermofisher Scientific, Waltham, MA, USA	Cat#17105041
Ethanol	VWR International, Radnor, PA, USA	Cat#20821321
Fetal Bovine Serum (FBS)	Thermofisher Scientific, Waltham, MA, USA	Cat#10270106

(*Continued on next page*)

Continued

REAGENT or RESOURCE	SOURCE	IDENTIFIER
Fuchsin	Bio Optica, Milan, IT	Cat#05-B10005
Glycerol	Sigma-Aldrich, St. Louis, MO, USA	Cat#G5516
Goat serum	Sigma-Aldrich, St. Louis, MO, USA	Cat#G9023
Ham's F10 Nutrient Mix	Thermofisher Scientific, Waltham, MA, USA	Cat#11550043
Horse serum	Thermofisher Scientific, Waltham, MA, USA	Cat#16050122
Hydrochloric acid	Sigma-Aldrich, St. Louis, MO, USA	Cat#30721
Iron hematoxylin Weigert - solution A	Bio Optica, Milan, IT	Cat#05-06008A/L
Iron hematoxylin Weigert - solution B	Bio Optica, Milan, IT	Cat#05-06008B/L
Penicillin-Streptomycin	Thermofisher Scientific, Waltham, MA, USA	Cat#15140122
Phosphomolibdic acid	Bio Optica, Milan, IT	Cat#05-M05003
Succinyl-acetone, 4–6 Dioxoheptanoic acid	Sigma Aldrich St. Louis, MO, USA	Cat#D1415
Sucrose	Sigma Aldrich St. Louis, MO, USA	Cat#S0389
Xylene	Sigma Aldrich St. Louis, MO, USA	Cat#247642
Critical commercial assays		
Purelink RNA mini kit	Thermofisher Scientific, Waltham, MA, USA	Cat#12183018A
High-Capacity cDNA Reverse Transcription Kit	Thermofisher Scientific, Waltham, MA, USA	Cat#4368813
Citrate Synthase Assay Kit	Sigma Aldrich, St. Louis, MO, USA	Cat#MAK193
Alpha Ketoglutarate (alpha KG) Assay Kit	Abcam, Cambridge, UK	Cat#ab83431
Malate Dehydrogenase Assay Kit	Sigma Aldrich, St. Louis, MO, USA	Cat#MAK196
Succinate Dehydrogenase Activity Colorimetric Assay Kit	BioVision, Milpitas, CA, USA	Cat#K660
Choline Assay Kit	Abcam, Cambridge, UK	Cat#ab219944
ATP Bioluminescent Assay Kit	Sigma-Aldrich, St. Louis, MO USA	Cat#FLAA
Hypoxyprobe^{TM} RED 549 Kit	Hypoxyprobe, Burlington, MA, USA	Cat#HP7-1000Kit
Choline Assay kit	Abcam, Cambridge, UK	Cat#ab219944
Experimental models: Cell lines		
Mouse: C2C12 cells	ATTC, Manassas, VA, USA	Cat#CRL-1772; RRID:CVCL_0188
Mouse: skeletal muscle satellite cells	isolated from muscle specific *Flvcr1a*$^{flox/flox}$ and *Flvcr1a*^{KO} mice (This paper)	N/A
Experimental models: Organisms/strains		
Mouse: *Flvcr1a*$^{fl/fl}$ mice	Vinchi et al.[14]	N/A
Mouse: *MyoD-iCRE* mice	Laboratory of Prof. Graziella Messina	Cat#014140; RRID:IMSR_JAX:014140
Mouse: *Flvcr1a*^{KO}: *Flvcr1a*$^{fl/fl}$;MyoD-iCre	This paper	N/A
Oligonucleotides		
Murine *ILoxFlvcr1* Fw: TCTAAGGCCCAGTAGGACCC	Vinchi et al.[14]	N/A
Murine *ILoxFlvcr1* Rev: GAAAGCATTTCCGTCCGCCC	Vinchi et al.[14]	N/A
Murine *IILoxFlvcr1* Rev: AGAGGGCAACCTCGGTGTCC	Vinchi et al.[14]	N/A
Murine *MyoD iCre* Fw: TGGGTCTCCAAAGCGACTCC	Kanisicak et al.[37]	N/A
Murine *MyoD iCre* Rev: GCGGATCCGAATTCGAAGTTCC	Kanisicak et al.[37]	N/A
Software and algorithms		
GraphPad Prism v9.0.0	GraphPad Software, Inc., La Jolla, CA, USA	https://www.graphpad.com/; RRID:SCR_002798
Fiji	Schindelin et al.[38]	http://fiji.sc/; RRID:SCR_002285

(*Continued on next page*)

Continued

REAGENT or RESOURCE	SOURCE	IDENTIFIER
Primer Express software v3.0	Thermofisher Scientific, Waltham, MA, USA	https://www.thermofisher.com/order/catalog/product/4363991/; RRID:SCR_014326

RESOURCE AVAILABILITY

Lead contact

Further information and requests for resources and reagents should be directed to and will be fulfilled by the Lead Contact, Emanuela Tolosano (emanuela.tolosano@unito.it).

Materials availability

All unique/stable reagents generated in this study will be made available on request, but we may require a payment and/or a completed Materials Transfer Agreement if there is potential for commercial application.

Data and code availability

- All data reported in this paper will be shared by the lead contact upon request.
- This paper does not report original code.
- Any additional information required to reanalyze the data reported in this paper is available from the lead contact upon request.

EXPERIMENTAL MODEL AND SUBJECT PARTICIPANT DETAILS

Primary cell cultures

Isolation of muscle satellite cells (SCs) by enzymatic dissociation was performed as previously described,[39] with minor modifications. Briefly, skeletal muscles (a mix of GS, TA, QD), obtained from the hind limbs of 5-month-old mice, were minced and incubated in 500 U/ml Collagenase II (Thermofisher Scientific, Waltham, MA, USA, catalog n° 17101015) in Ham's F10 medium (Thermofisher Scientific, Waltham, MA, USA, catalog n° 11550043) in a shaking incubator at 37°C for 40 min. The muscle digest was washed and resuspended in Wash Media (Ham's F10; 10% Horse Serum (Thermofisher Scientific, Waltham, MA, USA, catalog n° 16050122); 1% penicillin/streptomycin (Thermofisher Scientific, Waltham, MA, USA, catalog n° 15140122); 1% L-Glutamine (Thermofisher Scientific, Waltham, MA, USA) containing 200 U/ml Collagenase II (Thermofisher Scientific, Waltham, MA, USA, catalog n° 17101015) and 1.1/mL U Dispase (Thermofisher Scientific, Waltham, MA, USA, catalog n° 17105041), the resulting suspension was triturated with a pipet tip until the muscle is totally dissociated and placed in a shaking incubator at 37°C for 20 min. The muscle suspension was passed through 18 and 19-gauge needles using 10 mL syringes and filtered through 40 μm cell strainers. For isolation of MuSCs, muscles were stored for 12 h at 4°C before digestion. MuSCs were sorted using a FACSAria Fusion (BD Biosciences, Franklin Lakes, NJ, USA) by negative selection with antibodies recognizing CD31 FITC, CD45 FITC, F4/80 FITC (BD Biosciences, Franklin Lakes, NJ, USA) and Sca1-PE (Miltenyi Biotec, Bergisch Gladbach, Germany) (Lin −ve), and positive selection with an anti-alpha7 integrin PE-Vio770 (Miltenyi Biotec, Bergisch Gladbach, Germany) antibody, as previously described.[39] Cell viability was determined using 7-amino-actinomycin D (anti-7AAD, BD Biosciences, Franklin Lakes, NJ, USA) viability probe. After sorting 500 cells/cm2 mMuSCs were plated onto 0.2% w/v gelatin-coated Nunc 6-well plates (Thermofisher Scientific, Waltham, MA, USA) in proliferation medium composed of Ham F10 medium (Thermofisher Scientific, Waltham, MA, USA, catalog n° 11550043) supplemented with 20% FBS, 1% Chicken Embryo Extract (MP Biomedicals, Irvine, CA, USA, catalog n° 092850145). To induce myogenic differentiation, cells at 80% of confluence were plated in Dulbecco modified Eagle medium (DMEM, Thermofisher Scientific, Waltham, MA, USA) containing 2% horse serum (HS) for 7 days.

Cell lines

C2C12 cells (ATCC, Manassas, VA USA, catalog n° CRL-1772, RRID:CVCL_0188) were maintained in Dulbecco's modified Eagle's medium (DMEM, high glucose, GlutaMAX supplement; Gibco by Thermofisher Scientific, Waltham, MA USA, catalog n°61965059) supplemented with 10% heat-inactivated low-endotoxin fetal bovine serum (FBS; Gibco by Thermofisher Scientific, Waltham, MA USA, catalog n°10270106). Cell medium was ordinarily supplemented with antibiotics (100U/ml penicillin and 100μg/ml streptomycin; Gibco by Thermo Fisher Scientific, Waltham, MA USA, catalog n°15140122). Cells were maintained in a 37°C and 5% CO2 air incubator and routinely screened for absence of mycoplasma contamination.

Animal models

To generate muscle-specific *Flvcr1a* knock-out mice, mice expressing the Cre recombinase under the control of the muscle-specific MyoD promoter[40] (kindly provided by Prof. Graziella Messina) were crossed with *Flvcr1a*$^{fl/fl}$ mice.[14] Mice heterozygous for both the

MyoD-iCre carrying allele and the Flvcr1a-floxed allele were backcrossed with *Flvcr1a*$^{fl/fl}$ mice to obtain muscle-specific Flvcr1a knock-out animals (referred to as *Flvcr1a*^{KO}). *Flvcr1a*$^{fl/fl}$ mice were used as controls.

To stimulate heme biosynthesis, mice were administered 30 mg/kg of 5-Aminolevulinic acid hydrochloride (ALA, Sigma Aldrich, St. Louis, MO USA, catalog n°A3785) dissolved in physiological solution through gavage and analyzed 16 h later (for both heme dosage and assessment of myoglobin protein levels).

All the mice were provided with food and water *ad libitum*. Female and male mice were used for preliminary behavioral tests, showing comparable results (data not shown). All the other experiments were exclusively performed on male mice. Males were chosen to minimize confounding variables related to the estrous cycle phases, which can influence heme/iron metabolism. All experiments involving living animals conform to the relevant regulatory standards and were conformed to Italian law (D.L.vo 116/92). This work was authorized by the Italian Ministry of Health, authorization number 331/2022-PR (CC652.175, 30/05/2022).

METHOD DETAILS

RNA extraction and quantitative real-time PCR

RNA extraction and real-time quantitative reverse transcription PCR analyses were performed as described previously.[41] Briefly, total RNA was extracted using Purelink RNA mini kit (Thermofisher Scientific, Waltham, MA USA, catalog n° 12183018A). Between 500 and 1000ng of total RNA were transcribed into complementary DNA (cDNA) by High-Capacity cDNA Reverse Transcription Kit (Thermofisher Scientific, Waltham, MA USA, catalog n° 4368813). Real-time RT-qPCR was performed using gene-specific TaqMan Gene Expression Assays (Thermo Fisher Scientific Waltham, MA, USA), except for *Flvcr1a*. For *Flvcr1a*, specific primers and the probe were designed using Primer Express Software v3.0 (Thermofisher Scientific, Waltham, MA USA, https://www.thermofisher.com/order/catalog/product/4363991/; RRID:SCR_014326) and real-time RT-qPCR was performed using the TaqMan Fast Advanced Master Mix (Thermofisher Scientific, Waltham, MA USA, catalog n°4444557).

Real-time RT-qPCR were performed on a 7900HT Fast or QuantStudio 6 Flex Real-Time PCR System (Thermofisher Scientific, Waltham, MA USA) and analysis was performed on RQ Manager or QuantStudio Real-Time PCR software. Transcript abundance, normalized to 18s or actin beta mRNA expression is expressed as a fold increase over a calibrator sample.

Protein extraction and western blot

Proteins were extracted from frozen tissue powders which were lysed by rotation for 30 min at 4°C in homemade RIPA buffer (150mM NaCl, 50mM Tris-HCl pH 7.5, 1% Triton X-100, 0.5% Sodium deoxycholate, 0.1% SDS, 1mM EDTA). The buffer was freshly supplemented with 1mM phosphatase inhibitor cocktail (Sigma Aldrich, St. Louis, MO USA, catalog n° P0044), 1mM PMSF (Sigma Aldrich, St. Louis, MO USA, catalog n° 93482-50ML-F) and protease inhibitor cocktail (La Roche, Basel, CH, catalog n° 04693116001). The lysate was clarified by centrifugation for 10–20 min at 4°C. Protein concentration in the supernatant was assessed by Bradford assay. 15 to 40 μg proteins were loaded on Bio-Rad precast gel (Mini-PROTEAN TGX Stain-Free Gels, catalog n° 4568086). The revelation was assessed using the ChemiDoc Imaging System (Bio-Rad, Hercules, CA USA).

Mitochondria isolation for enzymatic assays

According to a previous work,[42] tissue samples were lysed in 0.5mL buffer A (50 mmol/L Tris, 100 mmol/L KCl, 5 mmol/L MgCl2, 1.8 mmol/L ATP, 1 mmol/L EDTA, pH 7.2), supplemented with protease inhibitor cocktail III [100 mmol/L AEBSF, 80 mmol/L aprotinin, 5 mmol/L bestatin, 1.5 mmol/L E−64, 2 mmol/L leupeptin and 1 mmol/L pepstatin (Merck KGaA, Darmstadt, DE)], 1 mmol/L phenylmethylsulfonyl fluoride (PMSF), 250 mmol/L NaF. Samples were clarified by centrifuging at 650 x g for 3 min at 4°C, and the supernatant was collected and centrifuged at 13,000 x g for 5 min at 4°C. The new supernatant was discarded, the pellet containing mitochondria was washed in 0.5mL buffer A and re-suspended in 0.25mL buffer B (250 mmol/L sucrose, 15 μmol/L K2HPO4, 2 mmol/L MgCl2, 0.5 mmol/L EDTA, 5% w/v bovine serum albumin). A 50μL aliquot was sonicated and used for the measurement of protein content. To confirm the presence of mitochondrial proteins in the extracts, 10 μg of each sonicated sample were subjected to SDS-PAGE and probed with an anti-porin antibody (Abcam, Cambridge, UK). The sonicated samples were used to measure the enzymatic activities of 5′-aminolevulinate synthase 1, pyruvate dehydrogenase, citrate synthase, α-ketoglutarate dehydrogenase, succinate dehydrogenase and malate dehydrogenase. The remaining unsonicated part was used to measure the electron transport chain (ETC) complexes I-IV activities.

Mitochondrial ATP content

ATP levels in mitochondria extracts were assessed by the ATP Bioluminescent Assay Kit (Sigma-Aldrich, St. Louis, MO USA, catalog n° FLAA). ATP was quantified as relative light units (RLU) and converted into nmol ATP/mg mitochondrial proteins, according to a calibration curve previously set.

Enzymatic activity

5′-aminolevulinate synthase 1 activity

ALAS1 activity was measured according to a previous work.[43] 10 μL of the reaction product were injected into a Waters Acquity ultra performance liquid chromatography (UPLC), equipped with a binary solvent manager, sample manager, photodiode array detector

(PDA), fluorescence detector, column heater and an Acquity UPLC BEH C18, 1.7 μM, 2.1 × 100 mm column. ALA-derivative was detected by setting the detector with excitation λ = 370 nm and emission λ = 460 nm, and the range of PDA scanner between 210 and 500 nm. The results were converted into nmol/min according to a previously set titration curve and expressed as nmol/min/mg mitochondrial proteins.

Glycolytic enzymes activities

Samples were homogenized using a Tissue Lyser II (Qiagen) and filtered through a 60 μm strainer to obtain a single-cell suspension. Cells were centrifuged at 1,200 x g for 5 min at room temperature and washed twice with PBS 1X, resuspended in 200 μL of 100 mM TRIS 10 mM/EDTA I mM (pH 7.4), and sonicated on ice with two 10 s bursts. Enzymatic activities were measured on 10 μL cell lysates, incubated for 5 min at 37°C. The protein content was measured using the BCA1 kit (Sigma Aldrich, St. Louis, MO USA, catalog n°71285-M). Aldolase and pyruvate kinase (PK) activities were measured by using the Aldolase Activity Colorimetric Assay Kit (Bio-Vision, Waltham, MA USA, catalog n°K665) and the Enzymatic Assay of Pyruvate Kinase kit (Sigma Aldrich, St. Louis, MO USA, catalog n°MAK072), respectively. The activity of phosphofructokinase-1 (PFK) assay was measured spectrophotometrically, as reported in a previous work.[44] The activities of glyceraldehyde 3-phosphate dehydrogenase (GAPDH), enolase and lactate dehydrogenase (LDH) were measured spectrophotometrically according to previous works.[45,46] For GAPDH, tissue lysate was incubated with 5 mM 3-phosphoglyceric acid, 1 U phosphoglycerate 3-kinase, 5 mM ATP and 2.5 mM NADH. For enolase, tissue lysate was incubated with 10 mM $MgCl_2$, 100 mM KCl, 1 mM 2-phosphoglyceric acid, 0.4 mM ADP, 6.8 U/mL PK, 9.9 U/mL LDH, 0.2 mM NADH. For LDH, tissue lysate was incubated with 5 mM NADH and 20 mM pyruvic acid. For all assays of glycolytic enzymes, the activities were monitored measuring the absorbance variation at 340 nm using a Synergy HTX 96-well microplate reader (Bio-Tek Instruments, Winooski, VT). The kinetics were linear throughout the measurement.

Pyruvate dehydrogenase, citrate synthase, α-ketoglutarate dehydrogenase, succinate dehydrogenase and malate dehydrogenase activities

The enzymatic activities of pyruvate dehydrogenase (PDH), citrate synthase, α-ketoglutarate dehydrogenase, succinate dehydrogenase and malate dehydrogenase were measured on 10 μg mitochondrial proteins using the Pyruvate dehydrogenase (PDH) Enzyme Activity Microplate Assay Kit (Abcam, Cambridge, UK, catalog n° ab109902), Citrate Synthase Assay Kit (Sigma Aldrich, St. Louis, MO USA), Alpha Ketoglutarate (alpha KG) Assay Kit (Abcam, Cambridge, UK), Malate Dehydrogenase Assay Kit (Sigma Aldrich, St. Louis, MO USA), Succinate Dehydrogenase Activity Colorimetric Assay Kit (BioVision, Milpitas, CA USA), as per manufacturer instructions.

Activity of mitochondrial ETC complexes I-IV

The activity of mitochondria respiration complexes was measured according to a previous work.[42]

Histological and immunofluorescence analysis

Gastrocnemius, soleus and tibialis anterior cryosections (10 μm thick) of 2 and 10-month-old mice were obtained from muscles directly frozen in liquid nitrogen cooled isopentane and stored at −80°C after collection. Slides were defrosted and incubated with hematoxylin for 4 min, then rinsed in deionized water and incubated in 1% eosin for 30 s. Finally, slides were incubated for 30 s in 80-90-100% ethanol solution for dehydration and in 100% xylene (Sigma-Aldrich, USA) for 1 min before mounting with DPX reagent (VWR International, USA) and coverslips. For the assessment of SDH activity, 0.54 g of sodium succinate (Carlo Erba, cat. 483555) and 0.02 g of NBT (Sigma cat. N6876-1G) were dissolved in 20 mL of a 0.2 M phosphate buffer. Slides were incubated 1h at 37°C prior to washing three times in deionized water. Slides were then dehydrated for 30 s in 80-90-100% ethanol solution for dehydration and in 100% xylene for 1 min before mounting with DPX reagent and coverslips. For COX activity staining, slides were incubated 1 h at room temperature in the incubating solution (0.2 M phosphate buffer, 0.2 M sucrose, cytochrome *c* and DAB, Sigma-Aldrich, USA). Slides were then rinsed in deionized water and dehydrated for 30 s in 80-90-100% ethanol solution, prior to incubation for 1 min in 100% xylene and mounting with DPX reagent and coverslips. Endothelium, laminin and myosin heavy chain isoforms were analyzed by immunofluorescence. For endothelium slides were fixed with 4% paraformaldehyde for 10 min, permeabilized with 0.3% Triton X-100 for 15 min and incubated with 10% donkey serum to block non-specific binding for 1 h and then incubated with the primary antibodies (overnight at 4°C) diluted in blocking solution. Fluorochrome-conjugated secondary antibodies were diluted in PBS and added for 1h at room temperature. Slides were then mounted with Prolong Gold Antifade Reagent with DAPI (Thermo Fisher, Carlsbad, CA). For myofiber types characterization, tissue cryosections were fixed in cold 1:1 ethanol-acetone solution for 3 min at RT, followed by 3 washes in PBS 1X, 5 min each. Slides were incubated for 1 h with a blocking solution of 5% goat serum in PBS 1X at RT, and then incubated with primary antibody for MyHC type IIB 2 h at RT. After 3 PBS 1X washes of 5 min, goat anti-mouse IgM 594 secondary antibody was diluted 1:100 in PBS 1X and added for 1h at RT. Slides were washed again three times with PBS 1X and incubated with primary antibody for MyHC type I and IIA overnight at 4°C. The day after, slides were washed three times in PBS 1X for 5 min each, prior to incubation with goat anti-mouse IgG 421 and goat anti-mouse IgG 488 both diluted 1:100 in PBS 1x for 40 min at 37°C. After three washes with PBS 1X, slides were incubated with laminin primary antibody 2 h at RT, then washed, and incubated with goat anti-rabbit IgG 647 secondary antibody 1:100 in PBS 1x for 40 min at 37°C. Finally, the slides were washed in PBS, then mounted with 1:1 PBS 1X-glycerol (Sigma-Aldrich, St. Louis, MO, USA) solution and coverslips. Primary antibodies were used at the following dilutions in blocking solution: CD31 1:50; isolectin 1:100, myosin heavy chain Type I BA-D5 1:50, myosin heavy chain Type IIa sc-71 1:50, myosin heavy chain Type IIb BF-F3 1:50, laminin 1:200. For antibodies details see the "Key Resources Table". A modified version of Gömöri trichrome staining was performed to evaluate

the percentage of regenerating area in CTX treated mice. Frozen sections were brought to RT and placed in preheated Bouin's Fluid (BF) at 56°C for 15 min. Slides were then cooled down to RT and rinsed in tap water. Equal volumes of Hematoxylin Weigert's Iron Part A and B (Bio-Optica, Milan S.p.A. Italy) were applied to tissue sections for 5 min at RT. After washing in deionized water, acid alcohol solution (0,5% HCl in ethanol) was applied to sections for 10 s, to stain cytoplasm, followed by acid fuchsin solution (Bio-Optica, Milan S.p.A. Italy) diluted 1:2 in deionized water for 5 min. Tissue sections were incubated with phosphomolybdic acid (Bio-Optica, Milan S.p.A. Italy) for 5 min to block the staining of all tissue components other than connective tissue fibers. Then, slides were incubated with 15% aniline blue solution (Bio-Optica, Milan S.p.A., Italy) for 5 min to stain collagen fibers. Finally, slides were washed in deionized water combined with 1% glacial acetic acid (Carlo Erba, Milan, Italy) and incubated for 45 s in 100% ethanol solution, for dehydration, followed by incubation in 100% xylene (Sigma-Aldrich, USA) for 1 min before mounting with DPX reagent (VWR International, USA) and coverslips.

For H&E, SDH activity staining, COX activity staining and Gömöri trichrome staining, images were captured by Leica microdissector (CTR6000) or Leica DM6. For endothelium and myofiber types images, Leica DMi8 fluorescence microscope was used. The number of the different fiber types was manually counted and myofibers CSA was manually calculated using the freehand selection and the area measurement tools in Fiji (https://fiji.sc/). Areas of positivity for Gömöri trichrome, SDH, COX staining and endothelium immunofluorescence were manually identified and selected in ImageJ based on fixed thresholds.

Muscle hypoxia

Skeletal muscle hypoxia was assessed as described previously.[47] Briefly, pimonidazole hydrochloride (60 mg/kg) was injected i.p. 90 min prior to dissection and followed by immunostaining with RED 549 dye-conjugated anti-pimonidazole mouse IgG1 monoclonal antibody (RED 549-MAb1) (Hypoxyprobe RED 549 Kit) on gastrocnemius cryosections. Images were acquired on a Leica TCS SP8 confocal microscope (Leica Microsystems) and analyzed on ImageJ.

Grip strength test

For the grip strength test, which measures the strength of the fore limbs, the BIOSEB grip strength apparatus (BIOSEB, Vitrolles, FR, catalog n° BIO-GS3) was used. Mice were forced to grip at the top of the inclined grid with the forelimbs and were gently pulled toward the bottom. To perform one trial, this movement was repeated three times and the maximum strength per gram was recorded. Following one initial training trial, mice underwent five consecutive trials each.

Kondziela's inverted screen test

Kondziela's inverted screen test, which measures the strength of fore and rear limbs, was performed on a homemade grid (43 × 43 cm wire mesh consisting of 12 mm squares of 1 mm diameter wire, surrounded by 4 cm deep wooden beading), built according to a previous work.[48] The grid was held at 40 cm height from a padded surface. Mice were hung on the inverted screen up to 1 min, and the latency time on the grid was recorded. Training was not required, as hanging is a usual behavior for mice. Mice underwent three trials and were allowed to rest for 5 min among each trial. Results were normalized on mice body weight.

Rotarod performance test

The rotarod performance test, which reflect motor coordination measured as time spent on a rotating rod, was performed according to[49] on a "Ugo Basile" apparatus (Ugo Basile srl, Varese, IT, model 760). Mice were trained for 2 min the day of the experiment, then subjected to three trials of maximum 5 min. Mice were allowed 5 min of rest between each trial. The maximum latency time for each trial was recorded. The experiment was repeated twice in two non-consecutive days.

Treadmill performance test

The test of endurance to exercise was performed on a BIOSEB treadmill (Cornellà, ES, catalog n° BX-TM2_2012915). A modified version of the protocols described in[50–52] was used, adjusting the speed to mice age. Mice underwent three training sessions before testing. In the first training session, mice run on the treadmill for 10 min at a constant speed of 13 cm/s. A shock grid mounted at the end of the treadmill delivered a 0.1 mA current to provide motivation for exercise. After two days, mice were trained again three times for 10 min at 20 cm/s, 25 cm/s and 30 cm/s and they were allowed to rest for 10 min between each training session. The current intensity was raised to 0.4 mA. Lastly, mice were trained after two days for 5 min at 25 cm/s the day of the test and allowed to rest for 10 min before starting the experiment. Mice run at 25 cm/s and the speed was increased by 4 cm/s every 3 min until a maximum speed of 41 cm/s. If the mouse was still running at this stage the grade was increased every 3 min by 5%. The test was stopped when the mouse rested on the shock grid at the back of the treadmill for 5 s, and the maximum time spent on the treadmill was recorded.

Electron microscopy

For ultrastructural studies, freshly collected muscle samples were fixed in 2.5% glutaraldehyde, 0.1 M cacodylate buffer, pH 7.4. After washing in the buffer, half the samples were incubated *en bloc* with Perls' Prussian blue solution for 40 min; this step was omitted in the remaining half of the samples. Then, samples were cut into 1 mm^3 blocks and post-fixed with 2% osmium tetroxide (OsO4) buffered with cacodylate, dehydrated through increasing concentrations of ethanol and embedded in EPON epoxy resin. Images

of ultrathin sections stained with uranyl acetate and lead citrate were obtained using a transmission electron microscope (EM 109, Zeiss).

Tissue iron content measurement by ICP-MS

Mice were anesthetized with a mix of Zoletil (tiletamine-zolazepam; Virbac S.r.l., Milano, IT) at a dose of 80 mg/kg body weight and Rompun (xylazine, Bayer AG, Leverkusen, DE) at a dose of 16 mg/kg body weight. Muscles were excised after transcardiac perfusion of mice with 0.1 mol/L phosphate-buffered saline (PBS), washed in PBS, blotted dry, weighted and stored at −80°C prior to analyses. Tissue perfusion with PBS was necessary to reduce background, considering the high amount of physiological iron present in blood. Iron content in mice organs was determined using inductively coupled plasma mass spectrometry (ICP-MS) (Element-2; Thermo-Finnigan, Rodano, MI, Italy). Muscle tissues were homogenized with a Teflon homogenizer prior to centrifugation at 800g for 10 min at 4°C. The supernatant was centrifuged at 8000g for 10 min and the resulting pellet was used as the crude mitochondrial fraction. The total and mitochondrial muscle samples were suspended in 2% nitric acid and heated at 80°C for 15 min to extract iron. Iron content was measured using ICP-MS (Agilent 7900). Denatured proteins were pelleted by centrifugation at 10,000g for 15 min, and the total protein amount used for iron normalization.

Tissue heme content measurement

Tissue heme concentration was measured using a fluorescence assay, as previously reported.[53] Briefly, GS from 2 to 4-month-old mice untreated or treated with 30 mg/kg 5-aminolevulinic acid for 16 h were harvested following intracardiac perfusion with 1x phosphate buffered saline (PBS), to minimize potential interference from blood heme in the subsequent assay, and then frozen.

For the analysis of heme content in total GS lysates, 10 μg of 2% w/v tissue homogenate in cold 1x PBS were collected, and PBS1x was added to reach a final volume of 50ul. Then, 500ul of 2M oxalic acid was added to each sample. Samples were heated at 95°C for 30 min to promote iron removal from heme. Fluorescence (wavelength: excitation 405 nm - emission 660–720 nm) of the resultant protoporphyrin was assessed on a Glomax Multi Detection System (Promega Corporation, Madison WI, USA). The endogenous protoporphyrin content (measured in parallel unheated samples in oxalic acid) was subtracted. Data were normalized to total protein concentration in each sample. Results were expressed as pmol of heme/mg total protein.

For the analysis of heme content in cytosolic and mitochondrial fractions, cellular fractionation into cytosol and intact mitochondria was done essentially following a modified version of a previously described method.[54] Briefly, about 50 mg of the muscle (derived from the same animal in which muscle total heme amount was quantified) was disrupted with pestle and mortar and resuspended in 1mL of RHM buffer (210 mM mannitol, 20 mM sucrose and 4 mM HEPES). Following a centrifugation at 1000 x g for 5 min at 4°C, the supernatant was discarded and one volume of permeabilizing buffer (0.1% (v/v) digitonin in RHM buffer) was added to the pellet. The resuspended pellet was incubated on ice for 5 min, then vortexed and incubated for an additional 5 min. The samples were then centrifuged at 700 x g for 5 min at 4°C. After separating the supernatant (S1) and the pellet (P1), the supernatant S1 was centrifuged for 20 min at 21,000 x g at 4°C, to obtain a new supernatant (S2) containing cytosolic proteins. Parallelly, the pellet P1 was washed one time with 1mL of RHM buffer and centrifuged at 16,000 x g for 5 min at 4°C. The obtained supernatant was discarded, and the new pellet (P2) was added with a 4:1 volume of lysis buffer (0.025M Tris, 0.15M NaCl, 0.01M EDTA, 1% NP-40, 5% w/v Glycerol, all adjusted to pH 7.4 and then added with protease inhibitors and phosphatase inhibitors the day of use). After being gently resuspended, the pellet P2 was incubated on ice for 10 min and finally centrifuged at 21,000 x g for 10 min at 4°C. The obtained supernatant (S3) contained crude mitochondrial extracts. 10ug of cytosolic and mitochondrial extracts were then processed to measure heme content with the oxalic acid method, as described above.

Tissue free choline content measurement

Tissue free choline concentration was measured using the Choline Assay Kit (Abcam, Cambridge, UK, catalog n° ab219944), as per manufacturer instructions. Briefly, GS tissue from 4-month-old mice were harvested and frozen. 20 mg of tissue were homogenized in 400 μl Assay Buffer (provided by the kit) and centrifuged at 2500 rpm for 5–10 min at 4°C. 50 μl of Choline Reaction Mix, supplied by the kit, were mixed with 50 μl of each sample's supernatant. Fluorescence measurements (excitation wavelength: 540 nm, emission wavelength: 590 nm) were taken 30 min following the addition of the Choline Reaction Mix. Non-specific fluorescence was subtracted, based on a parallel blank control. The choline concentration in each sample was calculated using a standard curve derived from a freshly prepared set of standards that were analyzed simultaneously.

Cardiotoxin treatment

Cardiotoxin (CTX) was injected to induce skeletal muscle damage and regeneration according to a previous work.[55] Three local consecutive injections, each one of 15 μL, of $7.5*10^{-6}$ M Cardiotoxin Gamma from Naja pallida snake venom (Latoxan, France) resuspended in 0.5% NaCl physiological saline solution, were intramuscularly administered into tibialis anterior muscles of 5 months old mice and samples were collected after 6 and 10 days.

Blood and serum analysis

Complete blood count was performed using an automated laser cell counter hematology system (Advia120 Hematology System; Siemens Diagnostics), and confirmed with IDEXX ProCyte DX analyser, to assess the following parameters: red blood cells (RBC,

106/μL), hemoglobin (Hb, g/dl), hematocrit (HCT, %). CPK analysis was performed on serum samples at the baseline and after CTX treatment in *Flvcr1a*$^{fl/fl}$ and *Flvcr1a*^{KO} mice with CPK kit (Cobas), according to manufacturer's instructions.

ALA and SA satellite cells treatment

Satellite cells isolated from mouse skeletal muscles were treated with ALA (5-Aminolevulinic acid hydrochloride, Sigma Aldrich, St. Louis, MO USA, catalog n° A3785) or SA (Succinyl-acetone, 4–6 Dioxoheptanoic acid, Sigma Aldrich St. Louis, MO USA, catalog n° D1415) for 7 days in differentiating medium (DM).

ALA and SA were freshly prepared by dissolution in DM at a concentration of 5mM and 0.5mM, respectively, and the medium with treatment was refreshed every 48 h.

All solutions were kept in the dark.

QUANTIFICATION AND STATISTICAL ANALYSIS

Sample size, mean and statistical details of experiments can be found in the figure legends.

Statistical analyses were conducted in GraphPad Prism v9.0.0 (GraphPad Software, Inc., La Jolla, CA USA, https://www.graphpad.com/; RRID:SCR_002798). No statistical method was used to predetermine sample size in studies.